Natural Killer Cell Dysfunction In Human Bladder Cancer Is Caused By Tissue-Specific Suppression of SLAMF6 Signaling

Adam M. Farkas[1#*], Michelle A. Tran[1], Dina Youssef[1], Sreekumar Balan[1], Jenna H. Newman[1], François Audenet[2], Harry Anastos[3], Ante Peros[1], Aparna Ananthanarayanan[1], Jorge Daza[4] , Elena Gonzalez-Gugel[1], Keerthi Sadanala[1] , Jakob Theorell[5], Matthew D. Galsky[1], Amir Horowitz[6], John P. Sfakianos[3*], Nina Bhardwaj[1,3,7*]

[1] Division of Hematology & Medical Oncology, Tisch Cancer Institute, Icahn School of Medicine at Mount Sinai, New York, NY, 10029, USA.
[2] Department of Urology, Hôpital Européen Georges-Pompidou, AP-HP.Centre – Université de Paris, Paris, France.
[3] Department of Urology, Icahn School of Medicine at Mount Sinai, New York, NY, 10029, USA.
[4] Department of Urology, Roswell Park Comprehensive Cancer Center, Buffalo, NY, 14203.
[5] Department of Medicine, Center for Infectious Medicine, Karolinska Institute, Stockholm, Sweden.
[6] Department of Oncological Sciences, Tisch Cancer Institute, Icahn School of Medicine at Mount Sinai, New York, NY, 10029, USA.
[7] Parker Institute of Cancer Immunotherapy.

[#] Lead Contact
[*] Corresponding authors: adam.farkas@mssm.edu or nina.bhardwaj@mssm.edu or john.sfakianos@mountsinai.org

Summary:

NK cells are innate lymphocytes critical for surveillance of viruses and tumors, however the mechanisms underlying NK cell dysfunction in cancer are incompletely understood. We assessed the effector function of NK cells from bladder cancer patients and found severe dysfunction in NK cells derived from tumors versus peripheral blood. While both peripheral and tumor-infiltrating NK cells exhibited conserved patterns of inhibitory receptor over-expression, this did not explain the observed defects in NK surveillance in bladder tumors. Rather, TME-specific TGF-β and metabolic perturbations such as hypoxia directly suppressed NK cell function. Specifically, an oxygen-dependent reduction in signaling through SLAMF6 was mechanistically responsible for poor NK cell function, as tumor-infiltrating NK cells cultured *ex vivo* under normoxic conditions exhibited complete restoration of function, while deletion of SLAMF6 abrogated NK cell cytolytic function even under normoxic conditions. Collectively, this work highlights the role of tissue-specific factors in dictating NK cell function, and implicates SLAMF6 signaling as a rational target for immuno-modulation to improve NK cell function in bladder cancer.

Keywords: NK cells, Bladder Cancer, Immune Exhaustion, TME, Single-cell RNASeq, Immuno-metabolism, Hypoxia, SLAMF6, TGF-β

41

42 **Introduction:**

43 Urothelial cell carcinoma, or bladder cancer (BCa) is the 6th most commonly diagnosed cancer
44 worldwide, resulting in 150,000 deaths annually[1]. Clinically, BCa is classified as non-muscle invasive
45 (NMI), muscle-invasive (MI), or metastatic, with each stage having different prognoses and treatment.
46 Patients with high-risk NMI are generally resected then treated with intravesical BCG, a live
47 attenuated preparation of *Mycobacterium bovis*, highlighting the amenability of bladder tumors to
48 respond to immunotherapy. More recently, subsets of patients with metastatic and locally-advanced
49 disease have benefited from T cell-centric, immune checkpoint blockade (ICB) using monoclonal
50 antibodies (mAb) interfering with the PD-1: PD-L1 axis. Despite this progress, the average response
51 rate for ICB is ~20-30% [2-7], highlighting the need to identify additional targets that improve response
52 rates. Natural Killer cells (NK) are innate lymphocytes critical for host defense against viral pathogens
53 and transformed cells [8-10]. Unlike T and B cells, NK cells lack a somatically recombined, antigen-
54 specific receptor. Instead, targets are generally recognized as cells that have down-regulated Class I
55 HLA, and up-regulated molecules associated with cellular stress [11-13]. NK cell function is further tuned
56 by integrating signals transmitted by a diverse array of activating and inhibitory receptors [13,14]. NK cell
57 effector functions include the production of inflammatory cytokines such as IFNγ and TNFα,
58 recruitment and maintenance of dendritic cells via production of CCL5, GM-CSF, FLT3-L and XCL1/2,
59 antibody-dependent cellular cytotoxicity (ADCC), and direct killing via release of cytolytic granules
60 containing perforin and granzymes[15] . The two major subsets of human NK cells differ in effector
61 function, with less mature $CD56^{bright}CD16^{-}$ NK cells responsible for most cytokine production, and
62 more mature $CD56^{dim}CD16^{+}$ cells having enhanced cytotoxic potential[16,17].

63

64 During cancer and chronic viral infection, T cells acquire a phenotype of immune exhaustion marked
65 by upregulation of inhibitory receptors including PD-1, CTLA-4, Tim-3 and TIGIT, and defined by
66 effector dysfunction[18]. However, whether a parallel process affects NK cells remains incompletely
67 understood. Additionally, there is little insight pertaining to differences in NK cell phenotype between
68 primary tumor and distal sites like peripheral blood. We have previously shown that NK cells from
69 peripheral blood (pbNK) up-regulate the inhibitory receptor Tim-3 in individuals with melanoma and
70 non-muscle-invasive BCa [14,19]. To characterize BCa-specific perturbations in NK cells more
71 comprehensively, particularly across peripheral blood and tumor, we analyzed tumor tissue and
72 peripheral blood mononuclear cells (PBMC) from a cohort of 68 BCa patients with either NMI and MI
73 disease. We found that, in contrast to circulating blood NK cells, NK cells in the tumor

microenvironment (TME) were functionally suppressed, and that TGF-β, and a hypoxia-dependent reduction in signaling through SLAM6 were responsible for this dysfunction. These results identify novel pathways of NK cell modulation that may have an impact on BCa progression, and that may be targetable to improve NK cell surveillance.

Results

Bladder cancer induces NK cell maturation in peripheral blood but not tumor

The frequency and composition of tumor-infiltrating leukocytes (TIL) in solid tumors differs across malignancies and often across patients with the same disease and clinical stage [20-22]. However, the frequency of tumor-infiltrating T cells, NK cells, and dendritic cells (DC) is correlated with improved response to immune checkpoint blockade and overall survival [23-26]. Tumors at distal sites can also influence the phenotype of immune cells in peripheral blood [19,27,28]. To determine if BCa alters the frequency of major immune lineages, we performed FACS analysis on the PBMC (NMI: n=30, MI: n=16, HD: n=17), and primary tumors (NMI: n=13, MI: n=22) of a cohort of patients that included 22 individuals from whom matched PBMC and tumor tissue was available (**Table S1**), (Gating strategy depicted in **Figure S1A-S1B).** There was no difference in the number of total number of PBMC/mL of blood in patients compared to healthy donors (HD) **(Figure 1A)**, nor in the total number of cells/mg tumor tissue across disease stage **(Figure 1B)**. However, the frequency of TIL, (live, $CD45^+$, singlets) was significantly lower in MI versus NMI tumors (**Figure 1C).**

NK cells were the second-most prevalent lineage identified in bladder tumors after T cells, comprising up to 25% of TIL in NMI tumors, but with significantly decreased infiltration of more advanced MI tumors where they comprised ~11% of TIL **(Figures 1D + 1E)**. Given the reported paucity of NK cells in normal bladder tissue[29,30] and additional work showing infiltration of NK cells into bladder tumors[31], these data suggest that NK cells recognize and infiltrate bladder tumors. Tumors, independent of stage, contained equivalent frequencies of monocytes **(Figure S1C**), dendritic cells (DC) **(Figure S1D**), B cells **(Figure S1E)**, and $CD4^+$ and $CD8^+$ T cells **(Figure S1F)**.

In peripheral blood there was a striking increase in the frequency of NK cells (pbNK) in BCa patients compared to HD, with NMI and MI patients having 2.4-fold and 2.2-fold increases respectively **(Figure 1F)**. This accumulation was driven by an increase in more mature $CD56^{dim}CD16^+$ cells, and a concomitant decrease in less mature, $CD56^{bright}CD16^-$ NK cells. This suggests that increases in NK

106 cell frequency and maturation in the periphery can be driven by a tumor at a distal site. BCa patient
107 peripheral blood had no difference in the frequency of monocytes **(Figure S1G)** or DC **(Figure S1H)**
108 compared to HD, but did have a significant reduction in the frequency of B cells in MI patients
109 compared to HD **(Figure S1I)**, and in $CD4^+$ T cells independent of disease stage **(Figure S1J)**.

110

111 Comparing NK cell subsets across tissue type revealed that tumor-infiltrating NK cells (tNK) are
112 significantly less mature than pbNK from either HD or patients based on expression of the maturation
113 marker CD16 **(Figure 1G)**. $CD16^+$ NK cells are considered as more cytolytic than $CD16^-$ cells[32-34]
114 suggesting that tNK cells are not optimal for tumor surveillance. Representative FACS plots of pbNK
115 from HD and BCa patients as well as tNK are shown in **Figure 1H**. Finally, there was a significant,
116 inverse correlation, between the frequency of NK and T cells within the same tumor, with T cells
117 being enriched in more advanced MI tumors **(Figure 1I)**. This suggests that NK and T cells may
118 respond differently to different TMEs associated with muscle invasion/non-invasion.

119

120 *Tumor-infiltrating NK cells are dysfunctional but not terminally so*

121 We next determined if there were differences in effector function between NK cells from BCa patients
122 and healthy donors via co-culture with K562 cells, a Class I HLA-deficient human leukemia cell line.
123 pbNK cells from BCa patients produced IFNγ and degranulated, as determined by expression of
124 LAMP-1, equivalently to pbNK cells from HD **(Figures 2A-2E)**. In contrast, tNK cells produced
125 significantly less IFNγ compared to pbNK cells from both HD and BCa patients, and they were
126 variably degranulated even in the absence of K562 targets **(Figures 2A-2E)**. Importantly, K562
127 targets were unable to elicit further degranulation **(Figures 2D + 2E)**. Additionally, tNK cells released
128 significantly less Granzymes A and B into culture supernatant after co-culture with K562 targets than
129 pbNK cells **(Figure 2F)**. These results demonstrate that tNK cells are highly dysfunctional, likely due
130 to repetitive degranulation within the tumor and additional TME-specific factors.

131

132 The dichotomy in effector function between pbNK and tNK cells suggested that suppressive elements
133 unique to the TME undermine NK cell tumor surveillance. The architecture of the TME supports
134 diverse suppressive strategies that can be mediated by soluble factors [35-38], cell-cell interactions[39,40],
135 and the creation of a metabolically hostile milieu[41,42] To determine if physical disruption of the bladder
136 TME ameliorated NK cell function, we dissociated tumor tissue, divided samples in half, and
137 assessed NK cell function immediately *ex vivo*, or after 4 days of culture in media containing low

138 doses of IL-2 (50U/mL) or IL-15 (1ng/nL) to ensure NK cell survival **(Figure 2G)**. Unexpectedly, NK
139 cells challenged with K562 targets after 4 days of this "rest" culture regained the ability to produce
140 IFNγ and TNFα, and to degranulate appropriately **(Figure 2H-2K)**. The variable LAMP-1 expression
141 observed in the absence of target cells *ex vivo* was also reduced to baseline, with LAMP-1 only
142 expressed after addition of target cells **(Figure 2H + 2Ks)**. These data suggest that tNK cells are not
143 terminally dysfunctional, and that a structured TME is required to undermine NK cell function.

144

145 *Inhibitory receptors expressed by tumor-infiltrating NK cells are detectable on NK cells in the*
146 *peripheral blood*

147 Immune Checkpoint Blockade (ICB) directed against Tim-3, TIGIT, and NKG2A is being evaluated in
148 clinical trials for various solid tumors (e.g. NCT04139902, NCT04995523, and NCT05162755) , and
149 anti-PD-1/PD-L1 mAbs are already approved for many cancers including BCa[2,3]. However, most
150 studies have focused on the effect of these mAbs in the context of relieving T cell exhaustion, despite
151 significant promiscuity in receptor expression by both T and NK cells [19,43-46]. To determine if NK cells
152 express Tim-3, TIGIT, and/or NKG2A in the context of BCa, and if expression explained NK cell
153 dysfunction in the tumor, we analyzed PBMC (NMI: n=30, MI: n=16, HD: n=17) and primary tumors
154 (NMI: n=13, MI: n=22) from an expanded cohort of BCa patients that included 24 individuals from
155 whom matched blood and tumor tissue were available. In bladder tumors we observed a stage-
156 specific increase in Tim-3 expression by NK cells from NMI to MI tumors, whereas TIGIT was
157 expressed equivalently regardless of disease stage (range 17-48%, **Figure 3A).** There was minimal
158 expression of PD-1 by tNK cells as expected[47] (range 2.7-5.9%, **Figure 3A)**. Identical expression
159 patterns for Tim-3 and TIGIT were also observed on tumor-infiltrating $CD4^+$ and $CD8^+$ T cells, though
160 PD-1 expression was higher than what was observed for NK cells ($CD4^+$ T cells: 18-25.2% $PD\text{-}1^+$,
161 $CD8^+$ T cells: 15.9-24.9% $PD\text{-}1^+$) **(Figure S2A)**.

162

163 In peripheral blood there was also a stage-specific increase in Tim-3 expression between NMI and MI
164 patients similar to that observed for tNK cells (1.6-fold), as well as over-expression compared to HD
165 pbNK cells (2.8-4.6-fold) (**Figure 3B).** TIGIT was also over-expressed by BCa pbNK cells relative to
166 HD NK cells (10.8-11.8-fold), though again as found for tNK cells, in a stage-independent manner
167 **(Figure 3B).** There was negligible PD-1 expression by pbNK cells **(Figure 3B)**. We observed similar
168 expression patterns for Tim-3 TIGIT and PD-1 by $pbCD4^+$ and $pbCD8^+$ T cells **(Figure S2B)**.

169 NKG2A is another inhibitory receptor recognizing HLA-E on target cells.[36,48].. Examination of NKG2A
170 in a subset of our cohort (HD PBMC: n=3, BCa PBMC: n=4, Tumor: n=7) revealed that tNK cells
171 significantly over-express NKG2A relative to pbNK cells from HD and BCa patients **(Figure 3C and**
172 **S2D) (Figure)**. tCD8^{+} T cells also over-expressed NKG2A relative to those in peripheral blood
173 **(Figure S2C + S2D)**.
174
175 The unique disease stage-specificity of Tim-3 expression by NK cells across tissue suggested that
176 pbNK cells may be useful as a readout of tumor invasiveness. Indeed, we found Tim-3 expression on
177 NK cells from matched blood and tumor to be directly correlated **(Figure 3D),** maintaining this
178 possibility. However, this correlation did not explain the dramatic difference in functional capacity
179 between NK cells from the periphery and tumor. . We therefore compared Tim-3 expression with the
180 ability of pbNK and tNK cells to produce IFNγ and degranulate. Increasing Tim-3 positivity was
181 inversely correlated with the ability to degranulate and produce IFNγ by pbNK cells **(Figure 3E),** but
182 not by tNK cells **(Figure 3F).** This suggests that over-expression of Tim-3 may be sufficient to
183 suppress NK cell function, but that in the bladder TME it is not necessary.

184

185 *Ex vivo blockade of Tim-3 enhances IFNy production and release of granzymes from NK cells in BCa*
186 *patient peripheral blood but not tumor*

187 Pre-clinical blockade of Tim-3 and TIGIT with mAbs has been reported as enhancing NK and T cell
188 function in mice and primary human cells [43,46,49-52]. We tested if this strategy would improve the
189 function of BCa pbNK and tNK cells by treating PBMC or dissociated tumor with commercially
190 available anti-Tim-3 and anti-TIGIT mAbs (Tim-3: F38-2E2, TIGIT: MBSA34, and 741170) for 1h prior
191 to, and during, K562 co-culture. Tim-3 blockade increased the frequency of total and CD56^{bright} IFNγ^{+}
192 pbNK cells compared to control IgG **(Figures S3A-S3C)**, had no effect on LAMP-1/degranulation
193 **(Figure S3A + S3D)**, but did enhance the release of Granzymes A and B **(Figure S3E)** .TIGIT
194 blockade did not enhance any functional readout, and blockade of both receptors simultaneously
195 resembled blockade of Tim-3 alone **(Figure S3F-S3H).** Importantly, blockade of neither receptor
196 improved the function of NK cells from tumor, suggesting that dysfunctional NK cells in the TME may
197 be marked by expression of inhibitory receptors, but their dysfunction is not caused by it.

198

199 *scRNASeq identifies distinct transcriptional differences between NK cells in peripheral blood versus*
200 *bladder tumors*

201 Having established that inhibitory receptor expression alone did not explain the severe dysfunction of
202 tumor-infiltrating NK cells we performed 3' single-cell RNA sequencing (scRNASeq) on live, $CD45^+$
203 cells sorted from the PBMC (n=7) and tumors (n=6) of BCa patients to identify the TME-specific
204 factors that suppress NK function **(Figure 4A and Table S3)**. As a comparison, HD NK cells were
205 negatively bead-isolated from HD PBMC (n=5) and also sequenced. Details pertaining to scRNASeq
206 QC are shown in **Figure S4A-S4C**. Single-cell libraries from all 18 samples, comprising 68,192
207 immune cells, were integrated using Seurat [53,54] to identify cell types common across tissue of origin
208 and disease state. Graph-based clustering resulted in 19 clusters at resolution 0.8 **(Figure S4D)**, with
209 18,762 cells from four clusters (3, 4, 10, and 13) annotated as NK cells using module scores derived
210 from published NK cell gene signatures[26,55-58] **(Figures S4E + S4F and Table S4)**. The NK cells were
211 sub-clustered against each other, resulting in 5 clusters of NK cells at resolution 0.2 for analysis
212 **(Figure 4B)**. These NK cells were derived from each of the three tissues examined (HD PBMC: 7,809
213 NK cells, BCa PBMC: 7,082 NK cells, and TIL: 3,871 NK cells **(Figure S4G)** and represented each of
214 the twelve individual donors **(Figure S4H) (Figure 4B)**. We then calculated the differentially
215 expressed genes (DEG) in the NK cells from each cluster, parsed by tissue of origin **(Figure 4C)**.
216 There was little overlap in gene expression by NK cells belonging to the same cluster but originating
217 in different tissues. For example, in all clusters, genes defining NK cell effector signaling (CD247),
218 and glycolysis (LDHA, ENO1), were significantly higher in HD pbNK cells compared to those from
219 BCa patients regardless of tissue. Conversely, gene expression by tNK cells was associated with
220 sustained activation (HLA-DRA), tissue-residency [59] (CD69[60] and RGS1[61]), cellular stress (heat shock
221 proteins, TSC22D3[62]), inhibition of signaling (NFKBI, DUSP1), and production of inflammatory
222 cytokines (CCL3, CCL4, IFNG), but with little expression of cytolytic genes. Finally, pbNK cells from
223 BCa patients were enriched in genes involved in lymphocyte trafficking (S1PR4, SELL), protein
224 synthesis (ribosomal genes), and effector function (GZMH), but also inhibitory receptors (KLRG1).
225 Importantly, this analysis allowed for identification of genes that may be specific to tNK cells, such as
226 AREG, HLA-DRA, RGS1[61] and CD69 **(Figure 4C)**, and revealed that both the presence of BCa, and
227 the tissue of origin, induce specific programs of NK cell gene expression.

228

229 To examine the influence of both BCa and tissue type on NK cell gene expression, we compared
230 significant DEG for NK cells according to tissue, **(Figure 4D)**, as well as by genes of interest **(Figure**
231 **4E)**. HD pbNK cells were significantly enriched in cytolytic (GNLY, CST7, FGFBP2, GZMB), and
232 glycolytic (LDHA, ENO1) transcripts compared to NK cells from BCa patients, regardless of tissue.
233 Patient pbNK cells expressed genes associated with cytoskeletal rearrangements and target cell

234 adhesion (SH3BGRL3[63], CD2[64]), Granzyme B-independent cytolytic activity (GZMH, GZMM),
235 translation (ribosomal genes), and chemotaxis (S1PR1[65], CX3CR1[66]) . In contrast, tNK cells
236 expressed a paucity of cytolytic genes, were highly activated (CD69, HLA-DRA), immature (CD56[bright]
237 signature[67]), imprinted with tissue residency[61,68] (CD69, CXCR6, ITGA1, ITGAE, RGS1), and had
238 higher expression of a cytokine module that included IFNG (IFNG, TNF, CCL5, XCL1/2, FLT3LG)
239 **(Figures 4C + 4E** and **Table S4**)

240

241 NK cell effector functions are directly linked to their ability to perform glycolysis [69-71]. The dearth of
242 glycolytic genes such as LDHA and ENO1, observed in patient versus HD NK cells (**Figures 4C +**
243 **4D**) prompted us to further examine metabolic perturbations in the bladder TME. Indeed, tNK cells
244 had significantly higher scores for gene signatures associated with hypoxia [72,73] and glucose
245 deprivation [74], as well as a lower glycolysis [75] score, compared to pbNK cells from both healthy
246 donors and BCa patients **(Figure 4F and Table S4)**. Notably, these aberrations in tNK cells coincided
247 with a lower cytotoxicity score [76], but higher expression of genes in a cytokine module comprised of
248 IFNG, TNF, XCL1/2, and FLT3LG **(Figure 4F)**. These data suggested that the impaired cytolytic
249 capacity of tNK cells might result from a sub-optimal metabolic milieu that is unique to the TME.

250

251 Given the general competence of pbNK cells we sought to determine if NK cells progress through a
252 linear trajectory of increasing dysfunction, beginning with pbNK cells from HD, and terminating in tNK
253 cells. Accordingly, we constructed single-cell pseudotime trajectories using Monocle[77]. This approach
254 identified a continuum of NK cell differentiation with pbNK cells from HD at one terminus, tNK cells at
255 the other, and pbNK cells from BCa patients in the middle **(Figure 4G)**. The expression of transcripts
256 enriched in the tumor (e.g. AREG (epidermal growth factor-like protein amphiregulin), HLA-DRA, and
257 IFNG) showed progressive up-regulation as pseudotime progressed, with low expression in healthy
258 peripheral blood, induction in BCa patient peripheral blood, and maximal expression in tumor **(Figure**
259 **4H)**. Conversely, transcripts such as LDHA, the DC chemo-attractant CCL5, and the cytolytic gene
260 perforin (PRF1), were maximally expressed in HD pbNK cells, declined in BCa pbNK cells, and
261 reached lowest expression in sub-populations of tNK cells **(Figure 4H)**.

262 Finally, we conducted pathway enrichment analysis using Enrichr[78], taking the top 100 significantly
263 DEG from NK cells in each tissue as input. Effector pathways associated with NK cell surveillance
264 (e.g. IFNγ, cytotoxicity, and lymphocyte-target cell interactions), as well as glycolysis were enriched in
265 pbNK cells from HD, but largely absent in NK cells from BCa patients **(Figure 4I)**. pbNK cells from

266 BCa patients were enriched in processes involving translation, focal adhesion, and regulation of the
267 actin cytoskeleton, likely representing activated, migratory cells that are not yet dysfunctional. Gene
268 expression by tNK cells was unique and involved processes associated with response to, and
269 production of, cytokines such as IL-12 and IFNγ, but also SMAD2/3 signaling downstream of TGF-β,
270 and phosphatase activity; two suppressive signatures that might underlie TME-specific NK cell
271 dysfunction. Taken together the tissue-specific conservation of NK cell transcriptional programs
272 mirrored the tissue-specific dysfunction we observed at the protein level. We chose to further
273 examine TGF-β signaling, glucose deprivation, and hypoxia as mechanistically underlying tNK cell
274 dysfunction because of their significance and specificity to the bladder TME.

275

276 *TGF-β suppresses NK cell effector function in bladder tumors*

277 TGF-β is a pleiotropic cytokine that mediates suppressive effects on multiple hematopoietic cells in
278 murine[79] and human BCa[23], including NK cells[59,80-84]. Because tNK cells were significantly enriched in
279 the SMAD2/3 pathway that is a hallmark of signaling through TGF-β **(Figure 4I)** we examined
280 expression of a gene set specifically comprising a TGF-β signaling signature, that was found to be
281 associated with poor response to PD-L1 blockade in BCa[23]. Indeed, tNK cells were significantly
282 enriched in gene expression downstream of TGF-β compared to pbNK cells regardless of BCa status
283 **(Figure 5A).** To confirm this we tested the ability of TGF-β to inhibit effector function in HD NK cells.
284 Culture of HD NK cells with 1ng/mL of IL-15 and TGF-β (.05ng/mL-50ng/mL) for 6 days significantly
285 reduced both IFNγ and LAMP-1 expression after co-culture with K562 targets **(Figures 5B-5C)**. To
286 increase phenotypic granularity we used the same culture system but performed CyTOF with an NK
287 cell-focused panel (Table S2) on HD PBMC (n=20). After acquisition, PBMC were clustered with
288 DepecheR[85], and 4 NK cell clusters were annotated. Clusters 1 and 2 showed a significant reduction
289 in IFNγ production and degranulation after exposure to TGF-β **(Figure 5D)**. TGF-β also inhibited IFNγ
290 production and degranulation elicited by Antibody-Dependent Cellular Toxicity (ADCC) by using Raji
291 cells coated with anti-CD20 as target cells instead of K562 **(Figure 5E)**. Cluster 1 NK cells were the
292 most susceptible to inhibition for both assays and both effector readouts. In addition to being the
293 largest Cluster, Cluster 1 NK cells expressed the most IdU (marking proliferative cells), CD56, Tim-3,
294 and CD94 (co-receptor for NKG2-family receptors) **(Figure 5F)**. Cluster 2 NK cells were the second-
295 most susceptible to TGF-β inhibition, and expressed the most Siglec-7, TIGIT and LILRB1, all
296 inhibitory receptors, as well as CD16. This suggests that TGF-β may inhibit effector functions both in
297 actively proliferating, less mature NK cells, as well as in more mature NK cells that have acquired an
298 inhibitory phenotype.

To validate whether TGF-β was explicitly detectable in BCa patients we performed O-link analysis to profile soluble proteins in patient plasma and cell-free urine. There was no difference in circulating TGF-β in BCa plasma across disease stage **(Figure 5G)**, but there was significantly more TGF-β in the urine of MI patients compared to NMI **(Figure 5G).** Urine cytology is used clinically to identify tumor cells during diagnosis and follow-up, and has recently been shown to contain immune cells that better resemble those found in bladder tumors that those from peripheral blood, presumably due to contact between urine and the tumor[86] (Tran and Bhardwaj *in revision).* While speculative, TGF-β in the TME likely acts to suppress NK cell function[81,87], may reduce NK cell efficacy via reprogramming into less cytolytic ILC1[88], and may contribute to the physical exclusion of NK cells from tumor nests as shown to occur for T cells in bladder tumors[23].

Hypoxia suppresses NK cell effector function in the bladder TME

The most striking differences in gene expression between pbNK cells and tNK were TME-specific metabolic disruptions such as defective glycolysis, hypoxia, and glucose deprivation **(Figure 4F)**. We sought to validate the latter two, using HD pbNK cells and the human IL-2-dependent NK cell line NK-92. First, we used the fluorescent glucose analog 2-NBDG to assess the ability of pbNK and tNK cells to uptake glucose. tNK cells had the ability to take up significantly more glucose than pbNK cells from both BCa patients and healthy donors **(Figure 6A)**. This suggests that the gene expression associated with glucose deprivation may reflect low levels of extracellular glucose in the TME rather than a defect in the ability to access it.

Gene expression associated with hypoxia was present almost exclusively in tNK cells **(Figure 4F)**. We performed IHC for HIF-1α on an FFPE tissue array containing sections of kidney, ureter, bladder, and stomach tumors, as well as normal tissue from those organs. HIF-1α^+ cells were present in all tumor sections but not normal tissue **(Figure 6B)** confirming the scRNAseq data. Next, we isolated HD pbNK cells and cultured them at 21% or 4% O_2 for 3-4 days prior to co-culture with K562 targets and assessed their function. Hypoxic HD NK cells had significant reductions in IFNγ production and degranulation compared to those in normoxic culture **(Figures 6C-6F)**. Hypoxia also suppressed the ability of HD pbNK cells to degranulate **(Figure 6G)** and produce TNFα **(Figure 6H)** in response to Antibody Dependent Cellular Cytotoxicity (ADCC). Having confirmed that that low extracellular O_2 in

330 the TME inhibits NK cell surveillance, we next sought to determine the molecular mechanism by
331 which this occurs.

332

333 *A hypoxia-induced defect in SLAMF6 signaling suppresses NK cell effector function in bladder tumors*

334 To identify changes in NK cell signaling that occur during hypoxia we used a dot blot array to detect
335 changes in the phosphorylation status of 59 relevant receptors containing ITAM/ITIM/ITSM
336 (Immunoreceptor Tyrosine Activating/Inhibitory/Switch Motif). Bead-isolated HD NK cells were
337 cultured at 21% or 4% O_2 for 3-4 days and used to make protein lysates before incubation with
338 capture Abs on the array, and subsequent probing with an HRP-conjugated anti-phospho-tyrosine Ab.
339 Hypoxic culture reduced signaling through multiple activating receptors such as NKp46, NKp80,
340 KIR2DL4, and DNAM-1 **(Figure 7A)**. However, the most striking difference was the reduction in
341 phosphorylation of the ITSM of SLAMF6 (Signaling Lymphocyte Activation Molecule 6) after hypoxic
342 culture **(Figures 7B + 7C).** SLAMF6 is a homotypic receptor (i.e., the ligand for SLAMF6 is also
343 SLAMF6) expressed by T, B, and NK cells[89]. It functions as an activating receptor in human NK cells
344 and mediates IFNγ production and degranulation via recruitment of the adaptor proteins SAP and
345 EAT-2 to its phosphorylated ITSM.[89-93] Importantly, when HD NK cells were cultured at 4% O_2 for 3-4
346 days, then "rested" at 21% O_2 for 3 days, phosphorylation of the ITSM of SLAMF6 was restored
347 **(Figures 7B + 7C),** analogous to the restoration of effector function observed after "rest" of tNK cells
348 from tumors. These data suggest that hypoxia suppresses both NK cell function and signaling
349 through SLAMF6, and that restoration of normoxia is accompanied by restoration of SLAMF6
350 signaling and NK cell function. Indeed, gene expression of SLAMF6, SH2D1A (SAP), SH2D1B (EAT-
351 2), PRF1 (Perforin), and GZMB (Granzyme B) were lowest in tNK cells, while tNK had the highest
352 expression of PTPN6 (SHP-1), a phosphatase involved in inhibition of SLAMF6 signaling[89] and
353 ZNF683, a zinc finger protein shown to inhibit transcription of EAT-2 and suppress NK cell
354 cytotoxicity[94] **(Figure7D)**. Together, these results implicate a hypoxia-induced inhibition of SLAMF6
355 signaling as underlying tNK cell dysfunction.

356

357 We next examined differences in gene expression between SLAMF6^{low} and SLAMF6^{high} NK cells in
358 our scRNAseq data. This revealed that SLAMF6^{low} NK cells lacked effector transcripts involved in
359 cytotoxicity (e.g. NKG7, GZMH, FCGR3A/CD16, and FGFBP2) compared to SLAMF6^{high} NK cells,
360 and therefore that SLAMF6 is important for proper cytolytic function (**Figure 7E).** To test this directly,
361 we used CRISPR to delete SLAMF6 in NK-92 cells, a human IL-2-dependent NK cell line, rather than

362 primary NK cells which are technically more challenging to modify. We first validated that NK-92 cells
363 were amenable to hypoxia-induced dysfunction analogously to primary NK cells and found that they
364 were **(Figure 7F)**. Using a Ribo Nucleo Protein (RNP) approach and nucleofection efficiently deleted
365 SLAMF6 at the protein level in NK-92 cells **(Figure 7G)**. Importantly, after co-culture of SLAMF6-KO
366 cells with K562 targets there was significantly less LAMP-1 and Granzyme B expression compared to
367 the mock control, confirming that an inability to signal through SLAMF6 compromises NK cell cytolytic
368 function **(Figure 7H + 7I)**. As a control, co-culture with K562 cells at 4% O_2 reduced degranulation by
369 WT NK-92 cells as expected, and resulted in a further, but minimal reduction by SLAMF-KO cells
370 **(Figure 7H)**. These results suggest that SLAMF6 is centrally involved in mediating NK cell cytolytic
371 activity.

372

373 To identify any global changes in gene expression that accompany deletion of SLAMF6, we
374 performed bulk RNAseq of WT or SLAMF6-KO NK-92 cells. SLAMF6-KO NK-92 cells showed
375 significant downregulation of genes involved in cytolytic activity (PRF1, GZMB, NKG7), glycolysis
376 (LDHA, ENO1, ALDOA1), and cytokines (CCL3, CCL5, IL32) **(Figure 7J)),** supporting our protein-
377 level results from *ex vivo* tNK cells **(Figure 2A-2F)**. Additionally, as RNAseq was performed on
378 normoxic NK-92 cells, it was notable that SLAMF6 positively regulated both cytolytic function and
379 glycolysis. This was further supported by pathway analysis of the significant DEG between WT and
380 KO NK-92 cells **(Figure 7K)**.

381

382 We also performed bulk RNAseq on HD NK cells cultured at 21% or 4% O_2 for 3 days to directly
383 query how hypoxia affects gene expression in primary NK cells. Hypoxic HD NK cells had significantly
384 less expression of cytokine (TNF, IFNG, XLC2) and cytolytic (GZMB) transcripts than normoxic cells
385 **(Figures 7L + 7M**) **,** supporting our functional results. Conversely, hypoxic HD NK cells were enriched
386 in genes involved in inhibitory signaling (KLRB1/CD161[95], VEGFA[96]) HIF-1α signaling, and glycolysis
387 **(Figures 7L + 7M)**, together describing a state of increased NK cell dysfunction in low oxygen, and
388 again in harmony with our previous observations.

389

390 We next queried publicly available datasets to determine if SLAMF6 expression was associated with
391 clinical outcomes[97,98]. Higher SLAMF6 expression was significantly correlated with longer
392 progression-free survival in BCa patients (n=187), and improved response to ICB across 13 solid
393 tumors including BCa, in a cohort of 1,160 individuals **(Figure 7N)**. Finally, a gene signature

394 combining hypoxia and TGF-β and inhibitory SLAMF6 signaling was most enriched in tNK cells
395 followed by BCa pbNK and HD pbNK cells **(Figure 7O and Table S4)**. This underscores the
396 contribution of all three TME-specific axes in undermining NK cell surveillance in bladder tumors.

397 **Discussion**

398 Our study provides the first comprehensive analysis of NK cell function in BCa patients, reveals
399 important differences between pbNK and tNK cells, and identifies SLAMF6 as a new translationally
400 relevant target for immunotherapy. We confirmed and expanded on previous work showing that
401 bladder tumors are substantially infiltrated by NK cells, and that pbNK cells from BCa patients have
402 no cytolytic impairment[31,99,100]. NK cells represented the second most abundant immune lineage after
403 T cells in NMI tumors, suggesting that they detect early perturbations associated with malignancy and
404 traffic to bladder tissue efficiently. We also observed a significant, inverse relationship between NK
405 cell infiltration and tumor invasiveness. This suggests that NK cells are important for controlling tumor
406 progression, but that increasing TGF-β, hypoxia, and defective signaling through SLAMF6 in the
407 TME, ultimately subvert this as tumors progress.
408
409 Up-regulation of inhibitory receptors such as PD-1 is a hallmark of T cell dysfunction in cancer[18]. We
410 identified a parallel process for NK cells that involved the inhibitory receptors Tim-3, TIGIT, and
411 NKG2A, all of which have been correlated with disease progression and decreased overall survival in
412 multiple cancers [101,102]. Tim-3 was over-expressed both by pbNK and tNK cells in a disease stage-
413 specific manner. This suggests that Tim-3^{+} pbNK cells have utility as a biomarker by which to assess
414 disease progression. Conversely, TIGIT was over-expressed by pbNK and tNK cells independent of
415 disease stage, making TIGIT^{+} NK cells useful as an indicator of the presence of BCa. These findings
416 validate and extend our previous work showing up-regulation of Tim-3 and TIGIT by pbNK cells in
417 NMI BCa patients[103].
418
419 However, Tim-3 and TIGIT expression alone could not explain the TME-specific dysfunction of tNK
420 cells. For example, while Tim-3 was expressed equivalently across both tissues, its expression was
421 only inversely correlated with impaired NK function in peripheral blood, not tumor. Additionally, while
422 *ex vivo* blockade of Tim-3 enhanced IFNy production and release of Granzymes A and B by pbNK
423 cells, there was no synergy when combined with TIGIT blockade, and neither improved tNK cell
424 function. Efforts to improve tNK cell function with a commercially available SLAMF6-Fc chimeric
425 protein, were not successful (Data not shown). One interpretation of these results is that commercial
426 clones simply do not block signaling through TIGIT. Indeed, multiple studies showing enhanced NK or

427 T cell function after TIGIT blockade have been conducted using murine cells[45,59] proprietary anti-
428 TIGIT Abs[46,59], combining TIGIT blockade with blockade of PD-(L)1[59,104,105], and/or humanized anti-
429 TIGIT Abs (REF). Alternatively, the lack of efficacy of both Abs for tNK cells may reflect a lack of
430 ligand expression in the TME or an inability of Ab-based blockade to overcome suppression imprinted
431 by the bladder TME, mediated by hypoxia, glucose deprivation, TGF-β- signaling, and likely other
432 factors.
433

434 To determine what caused TME-specific NK cell dysfunction, barring inhibitory receptor expression,
435 we performed scRNAseq of matched BCa PBMC and TIL, as well as HD pbNK cells. While tNK cells
436 were significantly enriched in transcripts associated with activation (CD69, HLA-DRA) and cytokine
437 production (IFNγ, TNFα, XCL1/2, FLT3LG), they were simultaneously enriched in genes involved in
438 TGF-β signaling (SMAD2/3), cellular stress, hypoxia, and glucose deprivation, as well as possessing
439 a gene signature implicating deficient signaling through SLAMF6. Indeed, metabolic dysregulation
440 and TGF-β in the TME have been shown to subvert cytolytic activity [106,107], and TGF-β specifically
441 can additionally convert tNK cells into poorly cytolytic Type 1 innate lymphoid cells[88,108], as well as
442 directly suppress NK cell glycolysis and by extension, cytolytic function[109,110]. We validated the ability
443 of TGF-β to suppress IFNγ production and degranulation by HD pbNK cells, both in response to K562
444 targets as well as when triggered by ADCC. Specifically, the largest NK cluster comprised of less
445 mature, proliferative cells, was also the most sensitive to TGF-β. This implies that not only are most
446 NK cells sensitive to TGF-β-mediated suppression in the TME, but that impairment of this population
447 specifically would interfere with maturation towards a more cytolytic $CD16^+$ population, and possibly
448 reduce the number of NK cells in bladder tumors. These results, along with the increased amount of
449 LAP-TGF-β present in urine from MI patients compared to NMI, support a strong, TME-specific,
450 suppressive role for TGF-β in undermining tNK cell function in bladder cancer.
451

452 We also confirmed our scRNAseq data proposing hypoxia as a putative, TME-specific, inhibitor of NK
453 cell function. Hypoxic culture significantly suppressed IFNγ and TNFα production, and decreased
454 degranulation by competent pbNK cells in response to both K562 targets and elicited by ADCC. HIF-
455 1α was also detectable by IHC in bladder tumor but not normal bladder. Furthermore, hypoxia, even
456 in the absence of additional TME-specific suppressive axes like TGF-β and glucose deprivation,
457 suppressed signaling through multiple NK cell activating receptors such as DNAM-1, NKp46, NKp80,
458 and SLAMF6. While speculative, a global inability to translate activating signals from the TME into
459 effector function would have deleterious consequences for NK cell surveillance in bladder tumors.

These results support literature showing improved function and tumor clearance in HIF-1α$^{-/-}$ NK cells[111]. We also showed that deletion of SLAMF6 abrogated NK cytolytic activity and production of Granzyme B even under normoxic conditions, suggesting that SLAMF6 is critical to the ability of NK cells to kill. Combined with our results demonstrating significantly less signaling through SLAMF6 during hypoxic culture, this suggests that low extracellular O_2 alone may cripple the ability of NK cells to destroy tumor cell targets in the TME. Finally, deletion of SLAMF6 also impaired glycolytic processes, again, even under normoxic conditions, suggesting that it may have a role in NK cell metabolism as well as NK cell cytotoxicity. Alternatively, it may be that the inability to signal through SLAMF6 reduces glycolytic capacity which in turn limits cytolytic activity.

Importantly however, we observed normoxic levels of phosphorylation in the ITSM of SLAMF6 after "resting" hypoxic NK cells for several days in normoxic conditions. As we also observed restoration of all tNK cell effector functions after "resting" bladder tumor in normoxic conditions, it is likely that functional recovery from hypoxia is mediated by restoration of SLAMF6 signaling, as well as an overall increase in aerobic respiration While speculative, some degree of NK cell proliferation in "rested" tumor cultures, in response to the low IL-2 /IL-15 added, could result in the presence of functional daughter cells by the end of the "rest" period. However, we expect that restored signaling through SLAMF6 plays a more significant role, as protocols aimed at inducing NK proliferation typically use much higher cytokine concentrations, and expand NK cells over the course of weeks, not days[112-114].

As mentioned above, bulk RNAseq of SLAMF6-KO cells revealed that SLAMF6 was also required for normal glycolysis, which has not previously been reported to our knowledge. A recent study showed that stem-like, partially-exhausted LCMV-specific CD8 T cells that were HIF-1α$^{-/-}$, over-expressed SLAMF6[115] and *Tcf7*, suggesting that the inability to "detect" hypoxia maintained SLAMF6 expression. This is consistent with our observation that SLAMF6 expression decreases in the hypoxic TME. NK cells have higher basal rates of glycolytic activity than other lymphocytes so as to immediately respond to target cells[69,110]. The dramatic lack of cytolytic function in SLAMF6 KO cells is partially due to its described role in mediating NK effector function[89,91,93,116], but may also result from a role for SLAMF6 in modulating glycolysis.

Our results are consistent with work demonstrating that SLAMF6 functions as an activating receptor on human NK cells, with its deletion reducing NK killing of non-hematopoietic target cells[90], its

recognition of influenza hemagglutinin and subsequent induction of NK cell function[117], and the ability of rSLAMF6 to enhance NK cell proliferation and IFNγ production[118]. SLAMF6 expression by $CD8^+$ T cells also marks the proliferative, progenitor-exhausted, stem-like cells that contribute to response to PD-1 blockade[119,120], but has also been described as having both co-activating[121-123] and co-inhibitory function[122,124] in a context-dependent manner.

The clinical relevance of competent SLAMF6 signaling is suggested by the improved progression-free survival in BCa patients, and the improved response to ICB in individuals with various solid tumors including BCa, in those with higher rather than lower expression. While this data does not implicate SLAFM6 expression specifically on NK cells as being protective, SLAMF6 is overwhelmingly expressed by NK, T and B cell populations, so it is likely that higher expression confers at least a general advantage in tumor immunosurveillance.

This work reveals dramatic, tissue-specific differences in the function, gene expression, signaling, and amenability to ICB, of NK cells in the context of BCa. Additionally, we identified a novel mechanism by which hypoxia specifically suppresses NK cell function in the TME by abrogating signaling through SLAMF6. Interventions aimed at ameliorating the metabolically-hostile TME and enhancing signaling through pathways suppressed by it, will hopefully have translational benefit for patients with multiple types of solid tumors.

Acknowledgements

The authors thank the patients who generously agreed to participate in this study and are grateful for their contribution. We also thank the expertise and assistance of the Dean's Flow Cytometry and Microscopy Cores at Mount Sinai, Emily Mongeau, Ellen Fraga, Mavis Pancake, and Christopher Bare. This work was funded by NIH R01 CA201189 (N.B.), NIH R01 CA249175 (N.B.), T32 AI007605 (A.M.F.), T32 AI007647 (A.M.F.), and a Translational Team Science Award from the Department of Defense, CA181008 (N.B., J.P.S.).

Author Contributions

A.M.F. and N.B. conceptualized the study, designed the experiments, and acquired funding . A.M.F. performed experiments, analyzed data and wrote the manuscript. D.Y. designed and performed experiments and analyzed data. M.A.T. designed experiments and analyzed data. S.B., J.H.N., and M.D.G. conceptualized experiments. E.G.G., A.A., A.P. and K.S. performed experiments. J.P.S. provided clinical specimens and acquired funding. F.A, H.A., and J.D. provided clinical specimens. A.H. provided scRNASeq and CyTOF data for HD NK cells. J.T. analyzed CyTOF data. All authors read the final manuscript.

Declaration of Interests

N.B. is an advisor, consultant, or board member for Apricity, Carisma Therapeutics, CureVac, Genotwin, Novartis, Primevax, Rome Therapeutics, Tempest Therapeutics, and ATP, and has received research support from Dragonfly Therapeutics, Harbour Biomed, and Regeneron. A.H. receives research funding from Astra Zeneca and has served on advisory boards for Purple Biotech and UroGen. M.D.G. receives research funding from Bristol Myers Squibb, Novartis, Dendreon, Astra Zeneca, Merck, and Genentech , and has served as an advisory board member/consultant for Bristol Myers Squibb, Merck, Genentech, AstraZeneca, Pfizer, EMD Serono, SeaGen, Janssen, Numab, Dragonfly, GlaxoSmithKline, Basilea, UroGen, Rappta Therapeutics, Alligator, Silverback, Fujifilm, Curis, Gilead, Bicycle, Asieris, Abbvie, Analog Devices, Veracyte, Daiichi, and Aktis. A.M.F., M.A.T., D.Y., J.H.N., S.B., E.G.G., K.S., A.A. A.P., F.A, H.A., J.T., and J.P.S. declare no competing interests.

561
562
563
564 **Materials and Methods**

565 **Human specimens**

566 Informed consent was obtained from all patients prior to collection of whole blood, urine, and/or
567 primary tumor tissue under an IRB-approved, genitourinary biorepository protocol at the Tisch Cancer
568 Institute at Mount Sinai. Leukopaks from healthy volunteers were purchased from the New York
569 Blood Center. PBMC were isolated from patient blood via density gradient centrifugation. Briefly,
570 venous blood was collected into EDTA-coated vacutainers (BD Biosciences), diluted 1:2 with DPBS
571 (Gibco), and centrifuged over Ficoll-Paque Plus (GE Healthcare). PBMC were collected and washed
572 with DPBS prior to RBC lysis with ACK (Gibco). Freshly resected tumor tissue was disassociated
573 immediately or placed into tissue storage solution (Miltenyi) at 4° overnight. Tumor tissue was then
574 weighed and dissociated at 37°C with a GentleMACS using program 37C_h_TDK_2 and human
575 tumor dissociation kit reagents (Miltenyi). Cells were passed sequentially through 100μM, 70μM, and
576 40 μM mesh strainers and washed with DPBS prior to RBC lysis. All NK cell functional assays,
577 scRNASeq, and most immunophenotyping was conducted using fresh cells. Any remaining PBMC or
578 tumor cell suspensions were frozen at -80°C overnight in 90% FBS and 10% DMSO at a rate of -1°C
579 /minute using a Mr. Frostee (Thermo Fisher) prior to storage in vapor phase liquid nitrogen.

580

581 **Flow cytometry and antibodies**

582 PBMC and single-cell suspensions derived from primary tumor tissue were stained with a fixable
583 viability dye (Thermo Fisher) on ice for 20' in DPBS. Cells were washed and F_c receptors blocked for
584 10' on ice in cold FACS buffer (2% BSA, 1mM EDTA in DPBS). Surface molecules were stained in
585 FACS buffer on ice for 30' before washing and acquisition. For intracellular staining, cells were
586 additionally fixed, permeabilized, and stained using CytoFix/CytoPerm reagents (BD). Cells were
587 interrogated on LSR Fortessa, LSR Fortessa X-20, or Attune cytometers and FACSDiva v8.0.2
588 software. Data was analyzed with FlowJo v10.8.2 (BD), and statistics and plots generated using
589 Prism 9.5.0 (GraphPad). Antibodies were purchased from BioLegend, eBiosciences, Miltenyi and BD
590 Biosciences, clones indicated in parantheses: CD45 (HI30), CD3 (SK7), CD14 (63D3), CD19
591 (HIB19), CD16 (3G8), CD56 (NCAM 16.2), CD4 (RPA-T4), CD8 (RPA-T8), Tim-3 (F38-2E2), TIGIT
592 (MBSA43), PD-1 (EH12.2H7), CD107a (H4A3), Granzyme B (GB11), IFNγ (B27), TNFα (Mab11),

593 NKG2A (REA110), SLAMF6 (NT7), CD4 (RPA-T4), CD8 (RPA-T8), HLA-DR (L243), CD123 (6H6),
594 CD11c (Bu15), Sirpα (15-414), and Clec9a (8F9).
595
596
597 **NK cell functional assays**
598 PBMC or single cell suspensions from tumor tissue were obtained as described above. Cells were
599 cultured at 37°C overnight in 96 well, V-bottom plates at a density of .5-1*10^6 cells/well in complete
600 media (cRPMI) (RPMI containing 10% FBS, 1% penicillin-streptomycin, 1% L-glutamine, and 1% non-
601 essential amino acids) containing 5ng/mL IL-15 (Peprotech) to activate NK cells. The following
602 morning, K562 cells (ATCC) were added to cultures at an effector to target cell ratio of 5:1 in cRPMI
603 containing IL-15 in addition to monensin (2μM) and anti-CD107a (.2μg/mL). After 4h, cells were
604 stained for surface markers, washed, fixed and permeabilized using CytoFix/CytoPerm reagents (BD
605 Biosciences), followed by intracellular staining for IFNγ, TNFα, and Granzyme B (where shown). For
606 *ex vivo* blockade studies, low endotoxin, sodium-azide-free, functional grade anti-Tim-3 (F38-2E2)
607 and/or anti-TIGIT (MBSA34 or 741170) or control IgG1 was added to cultures at 10μg/mL for 1h at
608 37°C prior to the addition of K562 target cells. For selected experiments, parallel wells without added
609 monensin were used to collect supernatants after NK:K562 co-culture. These supernatants were
610 analyzed for secreted cytokines and cytolytic effector molecules by flow cytometry, using a
611 commercially available bead-based immunoassay (NK/CD8 Legendplex, Biolegend). For Antibody
612 Dependent Cellular Cytotoxicity (ADCC) assays Raji cells (ATCC) were used at a 5:1 E:T ratio in
613 place of K562 target cells, and non-fucosylated anti-CD20 mAb or non-fucosylated control IgG (both
614 InvivoGen) was added at 10ug/mL in the presence of anti-LAMP-1 for 4 hours, prior to staining for
615 flow.
616
617 **Tumor rest assays**
618 Single cell suspensions from tumor tissue were isolated as described above and plated in cRPMI
619 containing either 50U/mL IL-2 or 1ng/mL IL-15 (Peprotech) in 12-well culture plates. On day 2, cells
620 were centrifuged, and the media replaced with fresh cRPMI and IL-2 or IL-15. On day 4, cells were
621 centrifuged, and media replaced with fresh cRPMI containing 5ng/mL rhIL-15 to activate NK cells.
622 The following morning K562 cells were added to cultures to assess NK function as described above.
623
624 **Glucose uptake assays**
625 To measure the frequency of cells able to uptake glucose, PBMC or cells from dissociated tumor
626 were incubated in Krebs-Ringers-HEPES (KRH) for 15 min at 37°C, washed with KRH, then

627 resuspended in KRH containing 100uM of 2-NBDG, a fluorescent glucose analog (ThermoFisher).
628 For 10 min at 37°C. Cells were subsequently washed and stained with lineage markers to identify NK
629 and T cells, and the frequency of 2-NBDG$^+$ cells determined by flow cytometry.
630
631
632 **Hypoxia assays**
633 Hypoxic cell culture (4% O_2) was performed by enclosing the cell culture plate in a plastic pouch with
634 an O_2 scavenger pack and an O_2 meter (nBionix hypoxic cell culture kit, Bulldog Bio). After the
635 concentration inside the pouch fell to 4% O_2, the cell culture plate was clamped off from the O_2
636 scavenger pack and was placed inside a standard incubator for the duration of the experiment (3-4d).
637
638 **Phospho-protein arrays**
639 The proteome profiler human phosphoimunoreceptor array kit (R&D Systems) was used to determine
640 the phosphorylation status of the ITSM of SLAMF6, according to the manufacturer's protocol. Briefly,
641 cells were cultured under the conditions described, then harvested to make protein lysates. Total
642 protein concentration was measured using a standard Bradford assay (Pierce Detergent Compatible
643 Bradford Assay Kit, ThermoFisher), and 150ugs of total protein was incubated on membranes pre-
644 spotted with capture antibodies for 59 immune-related receptors. Lysates were incubated with
645 membranes overnight at 4°, washed, and probed with an anti-phosphotyrosine-HRP detection
646 antibody before standard chemiluminescent detection on film. Films were semi-quantified with
647 QuickSpots software (Ideal Eyes https://idealeyes.com/products/QuickSpots.php).
648
649 **O-link**
650 The Olink Immuno-Oncology panel was used to measure the amounts of 92 soluble proteins present
651 in healthy or BCa patient plasma and BCa patient urine. Plasma was collected by centrifuging whole
652 blood at 1,000g for 10' at 4°C and urine was centrifuged at 500g for 5' at 4°C to remove any cells
653 present. Each analyte was detected using a pair of antibodies, each containing complimentary
654 oligonucleotides, with quantification by quantitative reverse transcriptase quantitative polymerase
655 chain reaction (RT-qPCR). 1 µL of plasma or cell-free urine was added to 3 µL of an O-Link binding
656 buffer and incubated overnight at 4°C. The following morning an O-link PCR master mix was added to
657 each well and pre-amplified. For detection, 2.8 µL of pre-amplified product from each well was mixed
658 with 7.2 µL Olink detection mix, transferred to an Olink fluidic circuit, and run on a BioMark qPCR

659 instrument (Standard BioTools). Samples were run in singlet with recommended technical controls.
660 Detailed protocols are available on the Olink website (https://www.olink.com). QC and normalization
661 were done by Olink guidelines. Data was analyzed using the ΔΔCt method and an Olink normalized
662 protein expression manager, and read out on a log2 scale as NPX (normalized protein expression),
663

664

665 **CyTOF on HD PBMC**

666 Frozen HD PBMC (n=20) were obtained from an IRB approved protocol at the Karolinska Institute.
667 PBMC were thawed and recovered in complete RPMI overnight without exogenous cytokines before
668 being stimulated with either 1 ng/mL of IL-15 (Peprotech) or 1 ng/mL of IL-15+ 5 ng/mL TGF-β
669 (Peprotech) for 6 days, with media being replaced with fresh media containing the appropriate
670 cytokines every 2 days. After the 6-day culture PBMC were transferred to V-bottom plates and co-
671 cultured with K562 cells (ATCC) (E/T ratio, 10:1) for 4 hours at 37°C in the presence of 10ug/mL
672 brefeldin A and .5ug/mL of anti-LAMP-1 mAb. 15 minutes prior to the end of K652 co-culture the
673 media was replaced with media containing a 1:500 dilution of rhodamine viability dye (Standard
674 BioTools) for subsequent analysis by CyTOF. For ADCC assays PBMC were cultured as above, but
675 Raji cells with bound anti-human CD20-IgG1 mAb (BioLegend, clone QA20A02) were used as
676 targets. After K562 or Raji co-culture HD PBMC were washed twice with CyFACS buffer (DPBS
677 containing 2mM EDTA and 0.1% BSA), and cells from each donor were barcoded by staining with
678 anti-human CD45 mAb conjugated to 195Pt, 196Pt, 198Pt (clone HI30, Biolegend) or anti-human
679 B2m mAb conjugated to 195Pt, 196Pt, 198Pt (clone 2M2, Biolegend) antibodies. Samples were then
680 washed with CyFACS buffer, fixed with 1% PFA, resuspended in BD FACS Lyse solution, and stored
681 at -80°C until staining for intracellular proteins. The cells were thawed, washed in CyFACS buffer, and
682 centrifuged at 300g for 15 minutes at 4°C. Samples were then permeabilized with Maxpar Barcode
683 permeabilization buffer (Standard BioTools) and intracellular barcoding performed by staining with
684 anti-human CD45 mAb-conjugated to Pd104, Pd105, Pd106, Pd108 and Pd110 (Standard BioTools)
685 for 30min at R.T. Samples were then pooled, resuspended in permeabilization buffer (eBioscience)
686 and stained for intracellular targets using the panel described in **Table S2** for 30min at 4°C. Finally,
687 samples were washed, then incubated with intercalators conjugated to Ir191/Ir193 (Standard
688 BioTools) diluted 1:4,000 in PBS containing 1% formaldehyde for 30 minutes at R.T. Samples were
689 washed a final time then resuspended in CSM-Ir and kept at 4°C until acquisition on a Helios mass
690 cytometer (Standard BioTools).
691

692

693
694
695
696 **Analysis of CyTOF NK clusters with Depeche**
697 For the clustering analysis, one donor with fewer than 100 events in both TGF-stimulated and non-
698 stimulated samples was excluded. For the remaining samples, either all events, (for samples with
699 <500 total events) or 500 random events (for samples >500 total events) were used for clustering, so
700 as to minimize the influence of samples containing high cell numbers. For clustering, Determination of
701 Essential Phenotypic Elements of Cells in High-dimensional Entities" (DEPECHE) was used[85]. This is
702 a penalized, k-means-based method that automatically identifies the optimal cluster resolution by
703 iterative clustering with different penalties and Adjusted Rand Index (ARI) comparisons between the
704 results. It also penalizes non-informative markers on a per-cluster basis. With this method, 4 clusters
705 were identified as giving rise to an optimally reproducible and statistically interpretable model. After
706 this clustering step, all previously excluded cells were assigned to the 4 identified clusters so as to
707 enable the highest possible statistical power in subsequent analyses.
708
709 **Immunohistochemistry**
710 Tim-3, PD-1, and CD3: Serial 5μM FFPE sections were stained for CD3 (Clone D7A6E, Cell
711 Signaling Technology, 1ug/mL), Tim-3 (Clone D5D5RTM, Cell Signaling Technology, 2ug/mL) and
712 PD-1 (Clone NAT-105, Sigma 2ug/mL), with the first serial section reserved for H&E staining. Slides
713 were deparaffinized and rehydrated, followed by staining of CD3 and PD-1 w with a BenchMark Ultra
714 autostainer (Roche). Tim-3 was stained manually after heat-induced epitope retrieval using the "high
715 pressure" program on an electric pressure cooker (Cuisinart CPC-600) for 7 minutes in Tris-EDTA
716 buffer (pH 9.0). The primary Ab was incubated O/N at 4°. All targets were detected with HRP-
717 conjugated 2°Abs directed against the host species of each 1° Ab, followed by chromogenic
718 revelation with 3, 3-diaminobenzadine. Images were acquired under brightfield illumination on a Nikon
719 Eclipse Ti-s inverted microscope or a Pannoramic Flash 250 digital slide scanner (3D Histech).
720
721 HIF-1α: A commercially available human multiple tumor tissue microarray comprised of 6μM FFPE
722 sections of kidney, ureter, bladder, and stomach tumors, as well as unmatched normal tissue controls
723 was used for HIF-1α IHC (Novus Biologicals). A rabbit anti-human HIF-1α monoclonal Ab was used
724 (Clone 2443C, Novus, 1μg/mL). Slides were deparaffinized, rehydrated, and subjected to heat-
725 induced epitope retrieval using the "simmer" program on an electric pressure cooker (Cuisinart CPC-
726 600) for 20 minutes in High pH antigen retrieval solution (eBioscience). Primary Abs were incubated

727 O/N at 4°and detected with an HRP-conjugated 2°Ab (Vector Laboratories). Chromogenic revelation
728 was performed with 3, 3-diaminobenzadine (HIF-1α) and Vector Red (Nkp46). Images were acquired
729 under brightfield illumination on a motorized Zeiss Axioimager to acquire tiled images. The multiple
730 tumor tissue array was obtained from Novus.
731

732 **Sample preparation for scRNASeq**

733 BCa patients, live, CD45$^+$ singlets were FACS-sorted (BD FACSAria II, 100μM nozzle, 4° C) from either
734 Ficoll-isolated PBMC or freshly dissociated tumor tissue. Cells were sorted into DPBS + .04% BSA,
735 resuspended at 1000 cells/μL, and loaded onto a Chromium controller (10x Genomics) for
736 encapsulation into droplets, lysis, barcoding, reverse transcription, and library preparation using
737 Single Cell 3' v2 reagents. For HD NK cells, PBMC were isolated as above, followed by depletion of
738 non-NK lineages using immuno-magnetic beads (EasySep human NK cell enrichment kit, Stemcell
739 Technologies). Samples were sequenced in dedicated flow cells on a HiSeq 2500 (Illumina) to an
740 average depth of 91,787, 76,918, and 71,692 reads/cell for HD NK cells, BCa patient PBMC, and TIL
741 respectively.
742

743 **Pre-processing and analysis of scRNASeq**

744 Raw Illumina sequencing data was converted to FASTQ, demultiplexed and aligned to the GRCh38
745 reference genome using CellRanger v3.0.0 (10x Genomics). Subsequent analysis was performed
746 using Seurat v5[54] (https://satijalab.org/seurat) in RStudio v2021.09.0. For QC, cells expressing more
747 than 2,500, and fewer than 300 unique genes, as well as cells containing more than 10%
748 mitochondrial transcripts, were discarded. Genes expressed in fewer than 5 cells were also
749 discarded. Expression data was then normalized by a factor of 10,000 and log-transformed. Next,
750 highly variable genes in each sample were identified by binning the average expression and
751 dispersion of each gene using Seurat's FindVariableFeatures function. To enable direct comparisons
752 between NK cells from different tissues, disease stages, and donors, the resulting matrices from each
753 donor of HD PBMC NK cells (n=5), BCa PBMC (n=7), and TIL (n=6) were aligned and merged using
754 the FindIntegrationAnchors/IntegrateData approach in Seurat. Principal component analysis (PCA)
755 was run on the scaled data, and dimensionality reduction using UMAP was performed on the first 20
756 principal components. Next, graph-based clustering was performed, with iterative adjustment of the
757 resolution parameter in the FindClusters command to maximize cluster membership amongst donors.
758 Clusters were visualized using UMAP. Differentially expressed genes (DEG) were identified using a
759 non-parametric Wilcoxon rank sum test (Seurat FindMarkers and FindAllMarkers) on genes
760 expressed by ≥ 5% of cells with a ≥ 5% expression difference across the clusters being tested.

761 10,345 cells from TIL that were annotated as tumor, epithelial, stromal, or endothelial cells were
762 removed, resulting in a matrix comprised of 68,192 cells (7,812 HD NK cells, 39,963 PBMC, and
763 20,241 TIL) across 19 clusters at resolution .8. Of these, 18,762 cells in clusters 3, 4, 10, and 13 were
764 annotated as NK cells by comparing the module scores of published NK cell gene signatures
765 [26,55,57,125], as well as by expression of additional, canonical NK cell transcripts. These NK cell clusters
766 were then sub-clustered at resolution 0.2 to identify DEG across tissue and disease. Pathway
767 enrichment analysis was performed taking as input the top 100 significant DEG (by adjusted p-value)
768 for NK cells from each tissue as input. Pathways were queried using Enrichr [126]
769 (http://amp.pharm.mssm.edu/Enrichr) and visualized with GOPlot [127] and Prism v8. Gene signature
770 scores were calculated by subtracting the expression values of a randomly selected set of control
771 genes from that of the genes comprising each signature using the AddModuleScore function in
772 Seurat [128]. RNA pseudotime analysis was performed using Monocle v2.12 [77]. Briefly, NK cell genes
773 that were significantly differentially expressed across tissue and cluster of origin were used to order
774 cells in Monocle. Dimensionality reduction was performed using a max.components parameter of 4.
775
776

777 **SLAMF6 CRISPR in NK-92 cells**

778 NK-92 cells were cultured in Myelocult H5100 (StemCell Technologies) supplemented with 100U/mL
779 IL-2 (Peprotech). Low passage cells not exceeding $3*10^5$/mL were used for deletion of SLAMF6.
780 Briefly, SLAMF6 tracrRNA and crRNA (Alt-R CRISPR-Cas9 crRNA: 5'- /AI+R1/rGrGrU rUrUrC
781 rArUrG rGrGrG rUrArC rUrArU rGrArG rUrUrU rUrArG rArGrC rUrArUrGrCrU /AltR2/ -3', IDT) were
782 annealed to generate gRNA targeting SLAMF6. gRNA was incubated with Cas9 nuclease v3 (IDT)
783 and electroporation enhancer (IDT) to generate a Ribonucleoprotein (RNP). $5*10^5$ NK-92 cells were
784 resuspended in Solution 2 + Mannitol (5 mM KCl, 15 mM $MgCl_2$, 15 mM HEPES, 150 mM Na_2HPO_4
785 /NaH_2 containing 50 mM mannitol, pH 7.2)[129] and the RNP was added. Nucleofections were
786 performed in a volume of 20uL in cuvettes (Lonza) with Pulse Code CM-137 on an Amaxa 4D-
787 Nucloefector X (Lonza). Cells were recovered and expanded in NK MACS media (Miltenyi)
788 supplemented with 500U/mL IL-2. On d5-d7 SLAMF6$^-$ NK-92 were sorted on a FACSAria (BD
789 Biosciences) and allowed to expand again for 7-14 days prior to co-culture with K562 to assess
790 function. Typical d5-d7 deletion efficiency was ~70% and typical sort purity was >90%.
791

792 **Bulk RNAseq of SLAM6-KO and Hypoxic NK-92 cells**

793 Total RNA was extracted from $1*10^6$ WT or sorted SLAMF6-KO NK-92 cells using an RNA Micro Kit
794 (Zymo Research). After PolyA selection libraries were prepared and Illumina sequencing of 20-30

795 million paired-end reads performed. DESeq2 was used to identify DEG between WT and SLAMF6-
796 KO cells. 2,024 significantly DEG were identified with significance defined as a gene having an
797 adjusted p-value of < 0.05 and an absolute log2 fold change > 1 as determined by the Wald test.
798 Samples were sequenced and DEG determined by Genewiz, and volcano plots were generated using
799 the R package EnhancedVolcano (https://github.com/kevinblighe/EnhancedVolcano).
800

801 **SLAMF6 and clinical outcomes**

802 Kmplot.com was used to query the association between SLAMF6 expression and BCa patient PFS,
803 as well as ICB response across 13 cancers (www. Kmplot.com). Kmplot uses a manually-curated
804 dataset with expression and survival data being obtained from TCGA, GEO, and EGA. The queried
805 clinical cohort is divided into two groups based on expression of the queried gene. A Kaplan-Meier
806 plot is generated and the hazard ratio, 95% confidence interval, and logrank p-values are
807 computed[130].
808
809
810
811
812
813
814
815
816
817
818
819
820
821
822
823
824
825
826
827
828
829
830
831
832
833
834
835
836
837
838

1. Saginala, K., Barsouk, A., Aluru, J.S., Rawla, P., Padala, S.A., and Barsouk, A. (2020). Epidemiology of Bladder Cancer. Med Sci (Basel) *8*. 10.3390/medsci8010015.
2. Bellmunt, J., de Wit, R., Vaughn, D.J., Fradet, Y., Lee, J.L., Fong, L., Vogelzang, N.J., Climent, M.A., Petrylak, D.P., Choueiri, T.K., et al. (2017). Pembrolizumab as Second-Line Therapy for Advanced Urothelial Carcinoma. N Engl J Med *376*, 1015-1026. 10.1056/NEJMoa1613683.
3. Sharma, P., Retz, M., Siefker-Radtke, A., Baron, A., Necchi, A., Bedke, J., Plimack, E.R., Vaena, D., Grimm, M.O., Bracarda, S., et al. (2017). Nivolumab in metastatic urothelial carcinoma after platinum therapy (CheckMate 275): a multicentre, single-arm, phase 2 trial. Lancet Oncol *18*, 312-322. 10.1016/s1470-2045(17)30065-7.
4. Powles, T., O'Donnell, P.H., Massard, C., Arkenau, H.T., Friedlander, T.W., Hoimes, C.J., Lee, J.L., Ong, M., Sridhar, S.S., Vogelzang, N.J., et al. (2017). Efficacy and Safety of Durvalumab in Locally Advanced or Metastatic Urothelial Carcinoma: Updated Results From a Phase 1/2 Open-label Study. JAMA Oncol *3*, e172411. 10.1001/jamaoncol.2017.2411.
5. Rosenberg, J.E., Hoffman-Censits, J., Powles, T., van der Heijden, M.S., Balar, A.V., Necchi, A., Dawson, N., O'Donnell, P.H., Balmanoukian, A., Loriot, Y., et al. (2016). Atezolizumab in patients with locally advanced and metastatic urothelial carcinoma who have progressed following treatment with platinum-based chemotherapy: a single-arm, multicentre, phase 2 trial. Lancet *387*, 1909-1920. 10.1016/S0140-6736(16)00561-4.
6. Apolo, A.B., Infante, J.R., Balmanoukian, A., Patel, M.R., Wang, D., Kelly, K., Mega, A.E., Britten, C.D., Ravaud, A., Mita, A.C., et al. (2017). Avelumab, an Anti-Programmed Death-Ligand 1 Antibody, In Patients With Refractory Metastatic Urothelial Carcinoma: Results From a Multicenter, Phase Ib Study. J Clin Oncol *35*, 2117-2124. 10.1200/JCO.2016.71.6795.
7. Balar, A.V., Galsky, M.D., Rosenberg, J.E., Powles, T., Petrylak, D.P., Bellmunt, J., Loriot, Y., Necchi, A., Hoffman-Censits, J., Perez-Gracia, J.L., et al. (2017). Atezolizumab as first-line treatment in cisplatin-ineligible patients with locally advanced and metastatic urothelial carcinoma: a single-arm, multicentre, phase 2 trial. Lancet *389*, 67-76. 10.1016/S0140-6736(16)32455-2.
8. Smyth, M.J., Taniguchi, M., and Street, S.E.A. (2000). The Anti-Tumor Activity of IL-12: Mechanisms of Innate Immunity That Are Model and Dose Dependent. The Journal of Immunology *165*, 2665-2670. 10.4049/jimmunol.165.5.2665.
9. Gorelik, E., Wiltrout, R.H., Okumura, K., Habu, S., and Herberman, R.B. (1982). Role of NK cells in the control of metastatic spread and growth of tumor cells in mice. Int J Cancer *30*, 107-112.
10. Blois, S.M., Klapp, B.F., and Barrientos, G. (2011). Decidualization and angiogenesis in early pregnancy: unravelling the functions of DC and NK cells. J Reprod Immunol *88*, 86-92. 10.1016/j.jri.2010.11.002.
11. Habif, G., Crinier, A., Andre, P., Vivier, E., and Narni-Mancinelli, E. (2019). Targeting natural killer cells in solid tumors. Cell Mol Immunol *16*, 415-422. 10.1038/s41423-019-0224-2.
12. Algarra, I., Ohlen, C., Perez, M., Ljunggren, H.G., Klein, G., Garrido, F., and Karre, K. (1989). NK sensitivity and lung clearance of MHC-class-I-deficient cells within a heterogeneous fibrosarcoma. Int J Cancer *44*, 675-680.
13. Morvan, M.G., and Lanier, L.L. (2016). NK cells and cancer: you can teach innate cells new tricks. Nature Publishing Group *16*, 7-19.
14. da Silva, I.P., Gallois, A., Jimenez-Baranda, S., Khan, S., Anderson, A.C., Kuchroo, V.K., Osman, I., and Bhardwaj, N. (2014). Reversal of NK-cell exhaustion in advanced melanoma by Tim-3 blockade. Cancer immunology research.
15. Bhardwaj, N., Farkas, A.M., Gul, Z., and Sfakianos, J.P. (2020). Harnessing Natural Killer Cell Function for Genitourinary Cancers. Urol Clin North Am *47*, 433-442. 10.1016/j.ucl.2020.07.002.

16. Romagnani, C., Juelke, K., Falco, M., Morandi, B., D'Agostino, A., Costa, R., Ratto, G., Forte, G., Carrega, P., Lui, G., et al. (2007). CD56brightCD16- killer Ig-like receptor- NK cells display longer telomeres and acquire features of CD56dim NK cells upon activation. J Immunol *178*, 4947-4955. 10.4049/jimmunol.178.8.4947.
17. Freud, A.G., Mundy-Bosse, B.L., Yu, J., and Caligiuri, M.A. (2017). The Broad Spectrum of Human Natural Killer Cell Diversity. Immunity *47*, 820-833. 10.1016/j.immuni.2017.10.008.
18. Wherry, E.J., and Kurachi, M. (2015). Molecular and cellular insights into T cell exhaustion. Nature reviews. Immunology *15*, 486-499. 10.1038/nri3862.
19. Audenet, F., Farkas, A.M., Anastos, H., Galsky, M.D., Bhardwaj, N., and Sfakianos, J.P. (2018). Immune phenotype of peripheral blood mononuclear cells in patients with high-risk non-muscle invasive bladder cancer. World J Urol. 10.1007/s00345-018-2359-7.
20. Azizi, E., Carr, A.J., Plitas, G., Cornish, A.E., Konopacki, C., Prabhakaran, S., Nainys, J., Wu, K., Kiseliovas, V., Setty, M., et al. (2018). Single-Cell Map of Diverse Immune Phenotypes in the Breast Tumor Microenvironment. Cell *174*, 1293-1308 e1236. 10.1016/j.cell.2018.05.060.
21. Gubin, M.M., Esaulova, E., Ward, J.P., Malkova, O.N., Runci, D., Wong, P., Noguchi, T., Arthur, C.D., Meng, W., Alspach, E., et al. (2018). High-Dimensional Analysis Delineates Myeloid and Lymphoid Compartment Remodeling during Successful Immune-Checkpoint Cancer Therapy. Cell *175*, 1443. 10.1016/j.cell.2018.11.003.
22. Lavin, Y., Kobayashi, S., Leader, A., Amir, E.D., Elefant, N., Bigenwald, C., Remark, R., Sweeney, R., Becker, C.D., Levine, J.H., et al. (2017). Innate Immune Landscape in Early Lung Adenocarcinoma by Paired Single-Cell Analyses. Cell *169*, 750-765 e717. 10.1016/j.cell.2017.04.014.
23. Mariathasan, S., Turley, S.J., Nickles, D., Castiglioni, A., Yuen, K., Wang, Y., Kadel Iii, E.E., Koeppen, H., Astarita, J.L., Cubas, R., et al. (2018). TGFbeta attenuates tumour response to PD-L1 blockade by contributing to exclusion of T cells. Nature. 10.1038/nature25501.
24. Remark, R., Merghoub, T., Grabe, N., Litjens, G., Damotte, D., Wolchok, J.D., Merad, M., and Gnjatic, S. (2016). In-depth tissue profiling using multiplexed immunohistochemical consecutive staining on single slide. Sci Immunol *1*, aaf6925. 10.1126/sciimmunol.aaf6925.
25. Pages, F., Mlecnik, B., Marliot, F., Bindea, G., Ou, F.S., Bifulco, C., Lugli, A., Zlobec, I., Rau, T.T., Berger, M.D., et al. (2018). International validation of the consensus Immunoscore for the classification of colon cancer: a prognostic and accuracy study. Lancet *391*, 2128-2139. 10.1016/S0140-6736(18)30789-X.
26. Barry, K.C., Hsu, J., Broz, M.L., Cueto, F.J., Binnewies, M., Combes, A.J., Nelson, A.E., Loo, K., Kumar, R., Rosenblum, M.D., et al. (2018). A natural killer-dendritic cell axis defines checkpoint therapy-responsive tumor microenvironments. Nature medicine *24*, 1178-1191. 10.1038/s41591-018-0085-8.
27. Tallerico, R., Cristiani, C.M., Staaf, E., Garofalo, C., Sottile, R., Capone, M., Pico de Coana, Y., Madonna, G., Palella, E., Wolodarski, M., et al. (2017). IL-15, TIM-3 and NK cells subsets predict responsiveness to anti-CTLA-4 treatment in melanoma patients. Oncoimmunology *6*, e1261242. 10.1080/2162402X.2016.1261242.
28. Morita, T., Tokue, A., and Minato, N. (1990). Analysis of natural killer activity and natural killer cell subsets in patients with bladder cancer. Cancer immunology, immunotherapy : CII *32*, 191-194.
29. Yu, Z., Liao, J., Chen, Y., Zou, C., Zhang, H., Cheng, J., Liu, D., Li, T., Zhang, Q., Li, J., et al. (2019). Single-Cell Transcriptomic Map of the Human and Mouse Bladders. J Am Soc Nephrol. 10.1681/asn.2019040335.
30. Christmas, T.J. (1994). Lymphocyte sub-populations in the bladder wall in normal bladder, bacterial cystitis and interstitial cystitis. Br J Urol *73*, 508-515. 10.1111/j.1464-410x.1994.tb07635.x.

31. Mukherjee, N., Ji, N., Hurez, V., Curiel, T.J., Montgomery, M.O., Braun, A.J., Nicolas, M., Aguilera, M., Kaushik, D., Liu, Q., et al. (2018). Intratumoral CD56(bright) natural killer cells are associated with improved survival in bladder cancer. Oncotarget *9*, 36492-36502. 10.18632/oncotarget.26362.
32. Mandelboim, O., Malik, P., Davis, D.M., Jo, C.H., Boyson, J.E., and Strominger, J.L. (1999). Human CD16 as a lysis receptor mediating direct natural killer cell cytotoxicity. Proceedings of the National Academy of Sciences of the United States of America *96*, 5640-5644. 10.1073/pnas.96.10.5640.
33. Lanier, L.L., Yu, G., and Phillips, J.H. (1991). Analysis of Fc gamma RIII (CD16) membrane expression and association with CD3 zeta and Fc epsilon RI-gamma by site-directed mutation. J Immunol *146*, 1571-1576.
34. Mace, E.M. (2023). Human natural killer cells: Form, function, and development. J Allergy Clin Immunol *151*, 371-385. 10.1016/j.jaci.2022.09.022.
35. Donatelli, S.S., Zhou, J.M., Gilvary, D.L., Eksioglu, E.A., Chen, X., Cress, W.D., Haura, E.B., Schabath, M.B., Coppola, D., Wei, S., and Djeu, J.Y. (2014). TGF-beta-inducible microRNA-183 silences tumor-associated natural killer cells. Proceedings of the National Academy of Sciences of the United States of America *111*, 4203-4208. 10.1073/pnas.1319269111.
36. Mamessier, E., Sylvain, A., Thibult, M.L., Houvenaeghel, G., Jacquemier, J., Castellano, R., Goncalves, A., Andre, P., Romagne, F., Thibault, G., et al. (2011). Human breast cancer cells enhance self tolerance by promoting evasion from NK cell antitumor immunity. The Journal of clinical investigation *121*, 3609-3622. 10.1172/JCI45816.
37. Marvel, D., and Gabrilovich, D.I. (2015). Myeloid-derived suppressor cells in the tumor microenvironment: expect the unexpected. The Journal of clinical investigation.
38. Barrow, A.D., Edeling, M.A., Trifonov, V., Luo, J., Goyal, P., Bohl, B., Bando, J.K., Kim, A.H., Walker, J., Andahazy, M., et al. (2018). Natural Killer Cells Control Tumor Growth by Sensing a Growth Factor. Cell *172*, 534-548 e519. 10.1016/j.cell.2017.11.037.
39. Ferrari de Andrade, L., Tay, R.E., Pan, D., Luoma, A.M., Ito, Y., Badrinath, S., Tsoucas, D., Franz, B., May, K.F., Jr., Harvey, C.J., et al. (2018). Antibody-mediated inhibition of MICA and MICB shedding promotes NK cell-driven tumor immunity. Science *359*, 1537-1542. 10.1126/science.aao0505.
40. Guillerey, C., Huntington, N.D., and Smyth, M.J. (2016). Targeting natural killer cells in cancer immunotherapy. Nature immunology.
41. Lim, A.R., Rathmell, W.K., and Rathmell, J.C. (2020). The tumor microenvironment as a metabolic barrier to effector T cells and immunotherapy. Elife *9*. 10.7554/eLife.55185.
42. Vignali, P.D.A., DePeaux, K., Watson, M.J., Ye, C., Ford, B.R., Lontos, K., McGaa, N.K., Scharping, N.E., Menk, A.V., Robson, S.C., et al. (2023). Hypoxia drives CD39-dependent suppressor function in exhausted T cells to limit antitumor immunity. Nature immunology *24*, 267-279. 10.1038/s41590-022-01379-9.
43. Fourcade, J., Sun, Z., Pagliano, O., Chauvin, J.-M., Sander, C., Janjic, B., Tarhini, A.A., Tawbi, H.A., Kirkwood, J.M., Moschos, S., et al. (2014). PD-1 and Tim-3 regulate the expansion of tumor antigen-specific $CD8^+$ T cells induced by melanoma vaccines. Cancer Res. American Association for Cancer Research.
44. Chihara, N., Madi, A., Kondo, T., Zhang, H., Acharya, N., Singer, M., Nyman, J., Marjanovic, N.D., Kowalczyk, M.S., Wang, C., et al. (2018). Induction and transcriptional regulation of the co-inhibitory gene module in T cells. Nature *558*, 454-459. 10.1038/s41586-018-0206-z.
45. Johnston, R.J., Comps-Agrar, L., Hackney, J., Yu, X., Huseni, M., Yang, Y., Park, S., Javinal, V., Chiu, H., Irving, B., et al. (2014). The Immunoreceptor TIGIT Regulates Antitumor and Antiviral CD8(+) T Cell Effector Function. Cancer cell *26*, 923-937. 10.1016/j.ccell.2014.10.018.

46. Zhang, Q., Bi, J., Zheng, X., Chen, Y., Wang, H., Wu, W., Wang, Z., Wu, Q., Peng, H., Wei, H., et al. (2018). Blockade of the checkpoint receptor TIGIT prevents NK cell exhaustion and elicits potent anti-tumor immunity. Nature immunology. 10.1038/s41590-018-0132-0.
47. Judge, S.J., Dunai, C., Aguilar, E.G., Vick, S.C., Sturgill, I.R., Khuat, L.T., Stoffel, K.M., Van Dyke, J., Longo, D.L., Darrow, M.A., et al. (2020). Minimal PD-1 expression in mouse and human NK cells under diverse conditions. The Journal of clinical investigation *130*, 3051-3068. 10.1172/JCI133353.
48. Braud, V.M., Allan, D.S., O'Callaghan, C.A., Soderstrom, K., D'Andrea, A., Ogg, G.S., Lazetic, S., Young, N.T., Bell, J.I., Phillips, J.H., et al. (1998). HLA-E binds to natural killer cell receptors CD94/NKG2A, B and C. Nature *391*, 795-799. 10.1038/35869.
49. da Silva, I.P., Gallois, A., Jimenez-Baranda, S., Khan, S., Anderson, A.C., Kuchroo, V.K., Osman, I., and Bhardwaj, N. (2014). Reversal of NK-cell exhaustion in advanced melanoma by Tim-3 blockade. Cancer immunology research *2*, 410-422. 10.1158/2326-6066.CIR-13-0171.
50. Baghdadi, M., Nagao, H., Yoshiyama, H., Akiba, H., Yagita, H., Dosaka-Akita, H., and Jinushi, M. (2013). Combined blockade of TIM-3 and TIM-4 augments cancer vaccine efficacy against established melanomas. Cancer immunology, immunotherapy : CII *62*, 629-637. 10.1007/s00262-012-1371-9.
51. Sakuishi, K., Apetoh, L., Sullivan, J.M., Blazar, B.R., Kuchroo, V.K., and Anderson, A.C. (2010). Targeting Tim-3 and PD-1 pathways to reverse T cell exhaustion and restore anti-tumor immunity. The Journal of experimental medicine *207*, 2187-2194. 10.1084/jem.20100643.
52. Guillerey, C., Harjunpaa, H., Carrie, N., Kassem, S., Teo, T., Miles, K., Krumeich, S., Weulersse, M., Cuisinier, M., Stannard, K., et al. (2018). TIGIT immune checkpoint blockade restores CD8(+) T cell immunity against multiple myeloma. Blood. 10.1182/blood-2018-01-825265.
53. Stuart, T., Butler, A., Hoffman, P., Hafemeister, C., Papalexi, E., Mauck, W.M., 3rd, Hao, Y., Stoeckius, M., Smibert, P., and Satija, R. (2019). Comprehensive Integration of Single-Cell Data. Cell *177*, 1888-1902.e1821. 10.1016/j.cell.2019.05.031.
54. Butler, A., Hoffman, P., Smibert, P., Papalexi, E., and Satija, R. (2018). Integrating single-cell transcriptomic data across different conditions, technologies, and species. Nature Biotechnology *36*, 411. 10.1038/nbt.4096
https://www.nature.com/articles/nbt.4096#supplementary-information.
55. Crinier, A., Milpied, P., Escaliere, B., Piperoglou, C., Galluso, J., Balsamo, A., Spinelli, L., Cervera-Marzal, I., Ebbo, M., Girard-Madoux, M., et al. (2018). High-Dimensional Single-Cell Analysis Identifies Organ-Specific Signatures and Conserved NK Cell Subsets in Humans and Mice. Immunity *49*, 971-986.e975. 10.1016/j.immuni.2018.09.009.
56. Abbas, A.R., Baldwin, D., Ma, Y., Ouyang, W., Gurney, A., Martin, F., Fong, S., van Lookeren Campagne, M., Godowski, P., Williams, P.M., et al. (2005). Immune response in silico (IRIS): immune-specific genes identified from a compendium of microarray expression data. Genes Immun *6*, 319-331. 10.1038/sj.gene.6364173.
57. Newman, A.M., Liu, C.L., Green, M.R., Gentles, A.J., Feng, W., Xu, Y., Hoang, C.D., Diehn, M., and Alizadeh, A.A. (2015). Robust enumeration of cell subsets from tissue expression profiles. Nat Methods *12*, 453-457. 10.1038/nmeth.3337.
58. Balan, S., Arnold-Schrauf, C., Abbas, A., Couespel, N., Savoret, J., Imperatore, F., Villani, A.C., Vu Manh, T.P., Bhardwaj, N., and Dalod, M. (2018). Large-Scale Human Dendritic Cell Differentiation Revealing Notch-Dependent Lineage Bifurcation and Heterogeneity. Cell reports *24*, 1902-1915 e1906. 10.1016/j.celrep.2018.07.033.
59. Wienke, J., Visser, L.L., Kholosy, W.M., Keller, K.M., Barisa, M., Poon, E., Munnings-Tomes, S., Himsworth, C., Calton, E., Rodriguez, A., et al. (2023). Integrative analysis of

neuroblastoma by single-cell RNA sequencing identifies the NECTIN2-TIGIT axis as a target for immunotherapy. Cancer cell. 10.1016/j.ccell.2023.12.008.
60. Dogra, P., Rancan, C., Ma, W., Toth, M., Senda, T., Carpenter, D.J., Kubota, M., Matsumoto, R., Thapa, P., Szabo, P.A., et al. (2020). Tissue Determinants of Human NK Cell Development, Function, and Residence. Cell *180*, 749-763.e713. 10.1016/j.cell.2020.01.022.
61. Tang, F., Li, J., Qi, L., Liu, D., Bo, Y., Qin, S., Miao, Y., Yu, K., Hou, W., Li, J., et al. (2023). A pan-cancer single-cell panorama of human natural killer cells. Cell. 10.1016/j.cell.2023.07.034.
62. Quatrini, L., Wieduwild, E., Escaliere, B., Filtjens, J., Chasson, L., Laprie, C., Vivier, E., and Ugolini, S. (2018). Endogenous glucocorticoids control host resistance to viral infection through the tissue-specific regulation of PD-1 expression on NK cells. Nature immunology *19*, 954-962. 10.1038/s41590-018-0185-0.
63. Di Pisa, F., Pesenti, E., Bono, M., Mazzarello, A.N., Bernardi, C., Lisanti, M.P., Renzone, G., Scaloni, A., Ciccone, E., Fais, F., et al. (2021). SH3BGRL3 binds to myosin 1c in a calcium dependent manner and modulates migration in the MDA-MB-231 cell line. BMC Mol Cell Biol *22*, 41. 10.1186/s12860-021-00379-1.
64. Comerci, C.J., Mace, E.M., Banerjee, P.P., and Orange, J.S. (2012). CD2 promotes human natural killer cell membrane nanotube formation. PloS one *7*, e47664. 10.1371/journal.pone.0047664.
65. Walzer, T., Chiossone, L., Chaix, J., Calver, A., Carozzo, C., Garrigue-Antar, L., Jacques, Y., Baratin, M., Tomasello, E., and Vivier, E. (2007). Natural killer cell trafficking in vivo requires a dedicated sphingosine 1-phosphate receptor. Nature immunology *8*, 1337-1344. 10.1038/ni1523.
66. Ponzetta, A., Sciume, G., Benigni, G., Antonangeli, F., Morrone, S., Santoni, A., and Bernardini, G. (2013). CX3CR1 regulates the maintenance of KLRG1+ NK cells into the bone marrow by promoting their entry into circulation. J Immunol *191*, 5684-5694. 10.4049/jimmunol.1300090.
67. Salome, B., Gomez-Cadena, A., Loyon, R., Suffiotti, M., Salvestrini, V., Wyss, T., Vanoni, G., Ruan, D.F., Rossi, M., Tozzo, A., et al. (2019). CD56 as a marker of an ILC1-like population with NK cell properties that is functionally impaired in AML. Blood Adv *3*, 3674-3687. 10.1182/bloodadvances.2018030478.
68. Dogra, P., Rancan, C., Ma, W., Toth, M., Senda, T., Carpenter, D.J., Kubota, M., Matsumoto, R., Thapa, P., Szabo, P.A., et al. (2020). Tissue Determinants of Human NK Cell Development, Function, and Residence. Cell *180*, 749-763 e713. 10.1016/j.cell.2020.01.022.
69. Donnelly, R.P., Loftus, R.M., Keating, S.E., Liou, K.T., Biron, C.A., Gardiner, C.M., and Finlay, D.K. (2014). mTORC1-dependent metabolic reprogramming is a prerequisite for NK cell effector function. Journal of immunology (Baltimore, Md. : 1950) *193*, 4477-4484. 10.4049/jimmunol.1401558.
70. Assmann, N., O'Brien, K.L., Donnelly, R.P., Dyck, L., Zaiatz-Bittencourt, V., Loftus, R.M., Heinrich, P., Oefner, P.J., Lynch, L., Gardiner, C.M., et al. (2017). Srebp-controlled glucose metabolism is essential for NK cell functional responses. Nature immunology *18*, 1197-1206. 10.1038/ni.3838.
71. Mah, A.Y., Rashidi, A., Keppel, M.P., Saucier, N., Moore, E.K., Alinger, J.B., Tripathy, S.K., Agarwal, S.K., Jeng, E.K., Wong, H.C., et al. (2017). Glycolytic requirement for NK cell cytotoxicity and cytomegalovirus control. JCI insight *2*, e95128. 10.1172/jci.insight.95128.
72. Benita, Y., Kikuchi, H., Smith, A.D., Zhang, M.Q., Chung, D.C., and Xavier, R.J. (2009). An integrative genomics approach identifies Hypoxia Inducible Factor-1 (HIF-1)-target genes that form the core response to hypoxia. Nucleic Acids Research *37*, 4587-4602. 10.1093/nar/gkp425.
73. Makino, Y., Nakamura, H., Ikeda, E., Ohnuma, K., Yamauchi, K., Yabe, Y., Poellinger, L., Okada, Y., Morimoto, C., and Tanaka, H. (2003). Hypoxia-Inducible Factor Regulates Survival

of Antigen Receptor-Driven T Cells. The Journal of Immunology *171*, 6534. 10.4049/jimmunol.171.12.6534.

74. Ho, P.C., Bihuniak, J.D., Macintyre, A.N., Staron, M., Liu, X., Amezquita, R., Tsui, Y.C., Cui, G., Micevic, G., Perales, J.C., et al. (2015). Phosphoenolpyruvate Is a Metabolic Checkpoint of Anti-tumor T Cell Responses. Cell *162*, 1217-1228. 10.1016/j.cell.2015.08.012.
75. Moreno-Sanchez, R., Rodriguez-Enriquez, S., Saavedra, E., Marin-Hernandez, A., and Gallardo-Perez, J.C. (2009). The bioenergetics of cancer: is glycolysis the main ATP supplier in all tumor cells? Biofactors *35*, 209-225. 10.1002/biof.31.
76. Glimcher, L.H., Townsend, M.J., Sullivan, B.M., and Lord, G.M. (2004). Recent developments in the transcriptional regulation of cytolytic effector cells. Nature Reviews Immunology *4*, 900-911. 10.1038/nri1490.
77. Trapnell, C., Cacchiarelli, D., Grimsby, J., Pokharel, P., Li, S., Morse, M., Lennon, N.J., Livak, K.J., Mikkelsen, T.S., and Rinn, J.L. (2014). The dynamics and regulators of cell fate decisions are revealed by pseudotemporal ordering of single cells. Nature Biotechnology *32*, 381-386. 10.1038/nbt.2859.
78. Kuleshov, M.V., Jones, M.R., Rouillard, A.D., Fernandez, N.F., Duan, Q., Wang, Z., Koplev, S., Jenkins, S.L., Jagodnik, K.M., Lachmann, A., et al. (2016). Enrichr: a comprehensive gene set enrichment analysis web server 2016 update. Nucleic Acids Research *44*, W90-W97. 10.1093/nar/gkw377.
79. Yu, H., Sfakianos, J.P., Wang, L., Hu, Y., Daza, J., Galsky, M.D., Sandhu, H.S., Elemento, O., Faltas, B.M., Farkas, A.M., et al. (2022). Tumor-Infiltrating Myeloid Cells Confer De Novo Resistance to PD-L1 Blockade through EMT-Stromal and Tgfbeta-Dependent Mechanisms. Molecular cancer therapeutics *21*, 1729-1741. 10.1158/1535-7163.MCT-22-0130.
80. Wilson, E.B., El-Jawhari, J.J., Neilson, A.L., Hall, G.D., Melcher, A.A., Meade, J.L., and Cook, G.P. (2011). Human tumour immune evasion via TGF-beta blocks NK cell activation but not survival allowing therapeutic restoration of anti-tumour activity. PloS one *6*, e22842. 10.1371/journal.pone.0022842.
81. Viel, S., Marçais, A., Guimaraes, F.S.-F., Loftus, R., Rabilloud, J., Grau, M., Degouve, S., Djebali, S., Sanlaville, A., Charrier, E., et al. (2016). TGF-β inhibits the activation and functions of NK cells by repressing the mTOR pathway. Science Signaling *9*, ra19-ra19. 10.1126/scisignal.aad1884.
82. Regis, S., Dondero, A., Caliendo, F., Bottino, C., and Castriconi, R. (2020). NK Cell Function Regulation by TGF-beta-Induced Epigenetic Mechanisms. Frontiers in immunology *11*, 311. 10.3389/fimmu.2020.00311.
83. Kirschenbaum, D., Xie, K., Ingelfinger, F., Katzenelenbogen, Y., Abadie, K., Look, T., Sheban, F., Phan, T.S., Li, B., Zwicky, P., et al. (2023). Time-resolved single-cell transcriptomics defines immune trajectories in glioblastoma. Cell. 10.1016/j.cell.2023.11.032.
84. Ducimetiere, L., Lucchiari, G., Litscher, G., Nater, M., Heeb, L., Nunez, N.G., Wyss, L., Burri, D., Vermeer, M., Gschwend, J., et al. (2021). Conventional NK cells and tissue-resident ILC1s join forces to control liver metastasis. Proceedings of the National Academy of Sciences of the United States of America *118*. 10.1073/pnas.2026271118.
85. Theorell, A., Bryceson, Y.T., and Theorell, J. (2019). Determination of essential phenotypic elements of clusters in high-dimensional entities-DEPECHE. PloS one *14*, e0203247. 10.1371/journal.pone.0203247.
86. Wong, Y.N.S., Joshi, K., Khetrapal, P., Ismail, M., Reading, J.L., Sunderland, M.W., Georgiou, A., Furness, A.J.S., Ben Aissa, A., Ghorani, E., et al. (2018). Urine-derived lymphocytes as a non-invasive measure of the bladder tumor immune microenvironment. The Journal of experimental medicine *215*, 2748-2759. 10.1084/jem.20181003.

87. Zaiatz-Bittencourt, V., Finlay, D.K., and Gardiner, C.M. (2018). Canonical TGF-beta Signaling Pathway Represses Human NK Cell Metabolism. J Immunol *200*, 3934-3941. 10.4049/jimmunol.1701461.
88. Gao, Y., Souza-Fonseca-Guimaraes, F., Bald, T., Ng, S.S., Young, A., Ngiow, S.F., Rautela, J., Straube, J., Waddell, N., Blake, S.J., et al. (2017). Tumor immunoevasion by the conversion of effector NK cells into type 1 innate lymphoid cells. Nature immunology *18*, 1004-1015. 10.1038/ni.3800.
89. Dragovich, M.A., and Mor, A. (2018). The SLAM family receptors: Potential therapeutic targets for inflammatory and autoimmune diseases. Autoimmun Rev *17*, 674-682. 10.1016/j.autrev.2018.01.018.
90. Wu, N., Zhong, M.C., Roncagalli, R., Perez-Quintero, L.A., Guo, H., Zhang, Z., Lenoir, C., Dong, Z., Latour, S., and Veillette, A. (2016). A hematopoietic cell-driven mechanism involving SLAMF6 receptor, SAP adaptors and SHP-1 phosphatase regulates NK cell education. Nature immunology *17*, 387-396. 10.1038/ni.3369.
91. Eissmann, P., and Watzl, C. (2006). Molecular analysis of NTB-A signaling: a role for EAT-2 in NTB-A-mediated activation of human NK cells. J Immunol *177*, 3170-3177. 10.4049/jimmunol.177.5.3170.
92. Bottino, C., Falco, M., Parolini, S., Marcenaro, E., Augugliaro, R., Sivori, S., Landi, E., Biassoni, R., Notarangelo, L.D., Moretta, L., and Moretta, A. (2001). NTB-A [correction of GNTB-A], a novel SH2D1A-associated surface molecule contributing to the inability of natural killer cells to kill Epstein-Barr virus-infected B cells in X-linked lymphoproliferative disease. The Journal of experimental medicine *194*, 235-246. 10.1084/jem.194.3.235.
93. Perez-Quintero, L.A., Roncagalli, R., Guo, H., Latour, S., Davidson, D., and Veillette, A. (2014). EAT-2, a SAP-like adaptor, controls NK cell activation through phospholipase Cgamma, Ca++, and Erk, leading to granule polarization. The Journal of experimental medicine *211*, 727-742. 10.1084/jem.20132038.
94. Li, X., Chen, M., Wan, Y., Zhong, L., Han, X., Chen, X., Xiao, F., Liu, J., Zhang, Y., Zhu, D., et al. (2022). Single-cell transcriptome profiling reveals the key role of ZNF683 in natural killer cell exhaustion in multiple myeloma. Clin Transl Med *12*, e1065. 10.1002/ctm2.1065.
95. Pozo, D., Vales-Gomez, M., Mavaddat, N., Williamson, S.C., Chisholm, S.E., and Reyburn, H. (2006). CD161 (human NKR-P1A) signaling in NK cells involves the activation of acid sphingomyelinase. J Immunol *176*, 2397-2406. 10.4049/jimmunol.176.4.2397.
96. Cerdeira, A.S., Rajakumar, A., Royle, C.M., Lo, A., Husain, Z., Thadhani, R.I., Sukhatme, V.P., Karumanchi, S.A., and Kopcow, H.D. (2013). Conversion of peripheral blood NK cells to a decidual NK-like phenotype by a cocktail of defined factors. J Immunol *190*, 3939-3948. 10.4049/jimmunol.1202582.
97. Bartha, A., and Gyorffy, B. (2021). TNMplot.com: A Web Tool for the Comparison of Gene Expression in Normal, Tumor and Metastatic Tissues. Int J Mol Sci *22*. 10.3390/ijms22052622.
98. Fekete, J.T., and Gyorffy, B. (2019). ROCplot.org: Validating predictive biomarkers of chemotherapy/hormonal therapy/anti-HER2 therapy using transcriptomic data of 3,104 breast cancer patients. Int J Cancer *145*, 3140-3151. 10.1002/ijc.32369.
99. Tsujihashi, H., Matsuda, H., Uejima, S., Akiyama, T., and Kurita, T. (1989). Role of natural killer cells in bladder tumor. Eur Urol *16*, 444-449. 10.1159/000471637.
100. Carballido, J., Alvarez-Mon, M., Solovera, O.J., Menendez-Ondina, L., and Durantez, A. (1990). Clinical significance of natural killer activity in patients with transitional cell carcinoma of the bladder. J Urol *143*, 29-33. 10.1016/s0022-5347(17)39854-3.
101. Yang, M., Yu, Q., Liu, J., Fu, W., Cao, Y., Yu, L., Shao, S., Wang, X., Niu, H., and Wang, Y. (2015). T-cell immunoglobulin mucin-3 expression in bladder urothelial carcinoma: Clinicopathologic correlations and association with survival. J Surg Oncol *112*, 430-435. 10.1002/jso.24012.

102. Zhang, Y., Cai, P., Liang, T., Wang, L., and Hu, L. (2017). TIM-3 is a potential prognostic marker for patients with solid tumors: A systematic review and meta-analysis. Oncotarget *8*, 31705-31713. 10.18632/oncotarget.15954.
103. Audenet, F., Farkas, A.M., Anastos, H., Galsky, M.D., Bhardwaj, N., and Sfakianos, J.P. (2018). Immune phenotype of peripheral blood mononuclear cells in patients with high-risk non-muscle invasive bladder cancer. World J Urol *36*, 1741-1748. 10.1007/s00345-018-2359-7.
104. Banta, K.L., Xu, X., Chitre, A.S., Au-Yeung, A., Takahashi, C., O'Gorman, W.E., Wu, T.D., Mittman, S., Cubas, R., Comps-Agrar, L., et al. (2022). Mechanistic convergence of the TIGIT and PD-1 inhibitory pathways necessitates co-blockade to optimize anti-tumor CD8(+) T cell responses. Immunity *55*, 512-526 e519. 10.1016/j.immuni.2022.02.005.
105. Niu, J., Maurice-Dror, C., Lee, D.H., Kim, D.W., Nagrial, A., Voskoboynik, M., Chung, H.C., Mileham, K., Vaishampayan, U., Rasco, D., et al. (2022). First-in-human phase 1 study of the anti-TIGIT antibody vibostolimab as monotherapy or with pembrolizumab for advanced solid tumors, including non-small-cell lung cancer(☆). Ann Oncol *33*, 169-180. 10.1016/j.annonc.2021.11.002.
106. Chang, C.H., Qiu, J., O'Sullivan, D., Buck, M.D., Noguchi, T., Curtis, J.D., Chen, Q., Gindin, M., Gubin, M.M., van der Windt, G.J., et al. (2015). Metabolic Competition in the Tumor Microenvironment Is a Driver of Cancer Progression. Cell *162*, 1229-1241. 10.1016/j.cell.2015.08.016.
107. Viel, S., Marcais, A., Guimaraes, F.S., Loftus, R., Rabilloud, J., Grau, M., Degouve, S., Djebali, S., Sanlaville, A., Charrier, E., et al. (2016). TGF-beta inhibits the activation and functions of NK cells by repressing the mTOR pathway. Sci Signal *9*, ra19. 10.1126/scisignal.aad1884.
108. Crome, S.Q., Nguyen, L.T., Lopez-Verges, S., Yang, S.Y., Martin, B., Yam, J.Y., Johnson, D.J., Nie, J., Pniak, M., Yen, P.H., et al. (2017). A distinct innate lymphoid cell population regulates tumor-associated T cells. Nature medicine *23*, 368-375. 10.1038/nm.4278.
109. Cong, J., Wang, X., Zheng, X., Wang, D., Fu, B., Sun, R., Tian, Z., and Wei, H. (2018). Dysfunction of Natural Killer Cells by FBP1-Induced Inhibition of Glycolysis during Lung Cancer Progression. Cell Metab *28*, 243-255 e245. 10.1016/j.cmet.2018.06.021.
110. Sohn, H., and Cooper, M.A. (2023). Metabolic regulation of NK cell function: implications for immunotherapy. Immunometabolism (Cobham) *5*, e00020. 10.1097/IN9.0000000000000020.
111. Ni, J., Wang, X., Stojanovic, A., Zhang, Q., Wincher, M., Buhler, L., Arnold, A., Correia, M.P., Winkler, M., Koch, P.S., et al. (2020). Single-Cell RNA Sequencing of Tumor-Infiltrating NK Cells Reveals that Inhibition of Transcription Factor HIF-1alpha Unleashes NK Cell Activity. Immunity *52*, 1075-1087 e1078. 10.1016/j.immuni.2020.05.001.
112. Yang, Y., Badeti, S., Tseng, H.C., Ma, M.T., Liu, T., Jiang, J.G., Liu, C., and Liu, D. (2020). Superior Expansion and Cytotoxicity of Human Primary NK and CAR-NK Cells from Various Sources via Enriched Metabolic Pathways. Mol Ther Methods Clin Dev *18*, 428-445. 10.1016/j.omtm.2020.06.014.
113. Kloss, S., Oberschmidt, O., Morgan, M., Dahlke, J., Arseniev, L., Huppert, V., Granzin, M., Gardlowski, T., Matthies, N., Soltenborn, S., et al. (2017). Optimization of Human NK Cell Manufacturing: Fully Automated Separation, Improved Ex Vivo Expansion Using IL-21 with Autologous Feeder Cells, and Generation of Anti-CD123-CAR-Expressing Effector Cells. Hum Gene Ther *28*, 897-913. 10.1089/hum.2017.157.
114. Hennessy, R.J., Pham, K., Delconte, R., Rautela, J., Hodgkin, P.D., and Huntington, N.D. (2019). Quantifying NK cell growth and survival changes in response to cytokines and regulatory checkpoint blockade helps identify optimal culture and expansion conditions. Journal of leukocyte biology *105*, 1341-1354. 10.1002/JLB.MA0718-296R.
115. Wu, H., Zhao, X., Hochrein, S.M., Eckstein, M., Gubert, G.F., Knopper, K., Mansilla, A.M., Oner, A., Doucet-Ladeveze, R., Schmitz, W., et al. (2023). Mitochondrial dysfunction promotes

the transition of precursor to terminally exhausted T cells through HIF-1alpha-mediated glycolytic reprogramming. Nat Commun *14*, 6858. 10.1038/s41467-023-42634-3.

116. Chen, S., Yang, M., Du, J., Li, D., Li, Z., Cai, C., Ma, Y., Zhang, L., Tian, Z., and Dong, Z. (2016). The Self-Specific Activation Receptor SLAM Family Is Critical for NK Cell Education. Immunity. Elsevier Inc.
117. Duev-Cohen, A., Bar-On, Y., Glasner, A., Berhani, O., Ophir, Y., Levi-Schaffer, F., Mandelboim, M., and Mandelboim, O. (2016). The human 2B4 and NTB-A receptors bind the influenza viral hemagglutinin and co-stimulate NK cell cytotoxicity. Oncotarget *7*, 13093-13105. 10.18632/oncotarget.7597.
118. Flaig, R.M., Stark, S., and Watzl, C. (2004). Cutting edge: NTB-A activates NK cells via homophilic interaction. J Immunol *172*, 6524-6527. 10.4049/jimmunol.172.11.6524.
119. Miller, B.C., Sen, D.R., Al Abosy, R., Bi, K., Virkud, Y.V., LaFleur, M.W., Yates, K.B., Lako, A., Felt, K., Naik, G.S., et al. (2019). Subsets of exhausted CD8(+) T cells differentially mediate tumor control and respond to checkpoint blockade. Nature immunology *20*, 326-336. 10.1038/s41590-019-0312-6.
120. Schenkel, J.M., Herbst, R.H., Canner, D., Li, A., Hillman, M., Shanahan, S.L., Gibbons, G., Smith, O.C., Kim, J.Y., Westcott, P., et al. (2021). Conventional type I dendritic cells maintain a reservoir of proliferative tumor-antigen specific TCF-1(+) CD8(+) T cells in tumor-draining lymph nodes. Immunity *54*, 2338-2353 e2336. 10.1016/j.immuni.2021.08.026.
121. Gartshteyn, Y., Askanase, A.D., Song, R., Bukhari, S., Dragovich, M., Adam, K., and Mor, A. (2023). SLAMF6 compartmentalization enhances T cell functions. Life Sci Alliance *6*. 10.26508/lsa.202201533.
122. Hajaj, E., Zisman, E., Tzaban, S., Merims, S., Cohen, J., Klein, S., Frankenburg, S., Sade-Feldman, M., Tabach, Y., Yizhak, K., et al. (2021). Alternative Splicing of the Inhibitory Immune Checkpoint Receptor SLAMF6 Generates a Dominant Positive Form, Boosting T-cell Effector Functions. Cancer immunology research *9*, 637-650. 10.1158/2326-6066.CIR-20-0800.
123. Eisenberg, G., Engelstein, R., Geiger-Maor, A., Hajaj, E., Merims, S., Frankenburg, S., Uzana, R., Rutenberg, A., Machlenkin, A., Frei, G., et al. (2018). Soluble SLAMF6 Receptor Induces Strong CD8(+) T-cell Effector Function and Improves Anti-Melanoma Activity In Vivo. Cancer immunology research *6*, 127-138. 10.1158/2326-6066.CIR-17-0383.
124. Yigit, B., Wang, N., Ten Hacken, E., Chen, S.S., Bhan, A.K., Suarez-Fueyo, A., Katsuyama, E., Tsokos, G.C., Chiorazzi, N., Wu, C.J., et al. (2019). SLAMF6 as a Regulator of Exhausted CD8(+) T Cells in Cancer. Cancer immunology research *7*, 1485-1496. 10.1158/2326-6066.CIR-18-0664.
125. Balan, S., Arnold-Schrauf, C., Abbas, A., Couespel, N., Savoret, J., Imperatore, F., Villani, A.C., Vu Manh, T.P., Bhardwaj, N., and Dalod, M. (2018). Large-Scale Human Dendritic Cell Differentiation Revealing Notch-Dependent Lineage Bifurcation and Heterogeneity. Cell reports *24*, 1902-1915.e1906. 10.1016/j.celrep.2018.07.033.
126. Chen, E.Y., Tan, C.M., Kou, Y., Duan, Q., Wang, Z., Meirelles, G.V., Clark, N.R., and Ma'ayan, A. (2013). Enrichr: interactive and collaborative HTML5 gene list enrichment analysis tool. BMC Bioinformatics *14*, 128. 10.1186/1471-2105-14-128.
127. Walter, W., Sanchez-Cabo, F., and Ricote, M. (2015). GOplot: an R package for visually combining expression data with functional analysis. Bioinformatics *31*, 2912-2914. 10.1093/bioinformatics/btv300.
128. Tirosh, I., Izar, B., Prakadan, S.M., Wadsworth, M.H., 2nd, Treacy, D., Trombetta, J.J., Rotem, A., Rodman, C., Lian, C., Murphy, G., et al. (2016). Dissecting the multicellular ecosystem of metastatic melanoma by single-cell RNA-seq. Science *352*, 189-196. 10.1126/science.aad0501.

129. Rautela, J., Surgenor, E., and Huntington, N.D. (2020). Drug target validation in primary human natural killer cells using CRISPR RNP. Journal of leukocyte biology *108*, 1397-1408. 10.1002/JLB.2MA0620-074R.
130. Gyorffy, B. (2023). Discovery and ranking of the most robust prognostic biomarkers in serous ovarian cancer. Geroscience *45*, 1889-1898. 10.1007/s11357-023-00742-4.

Graphical Abstract

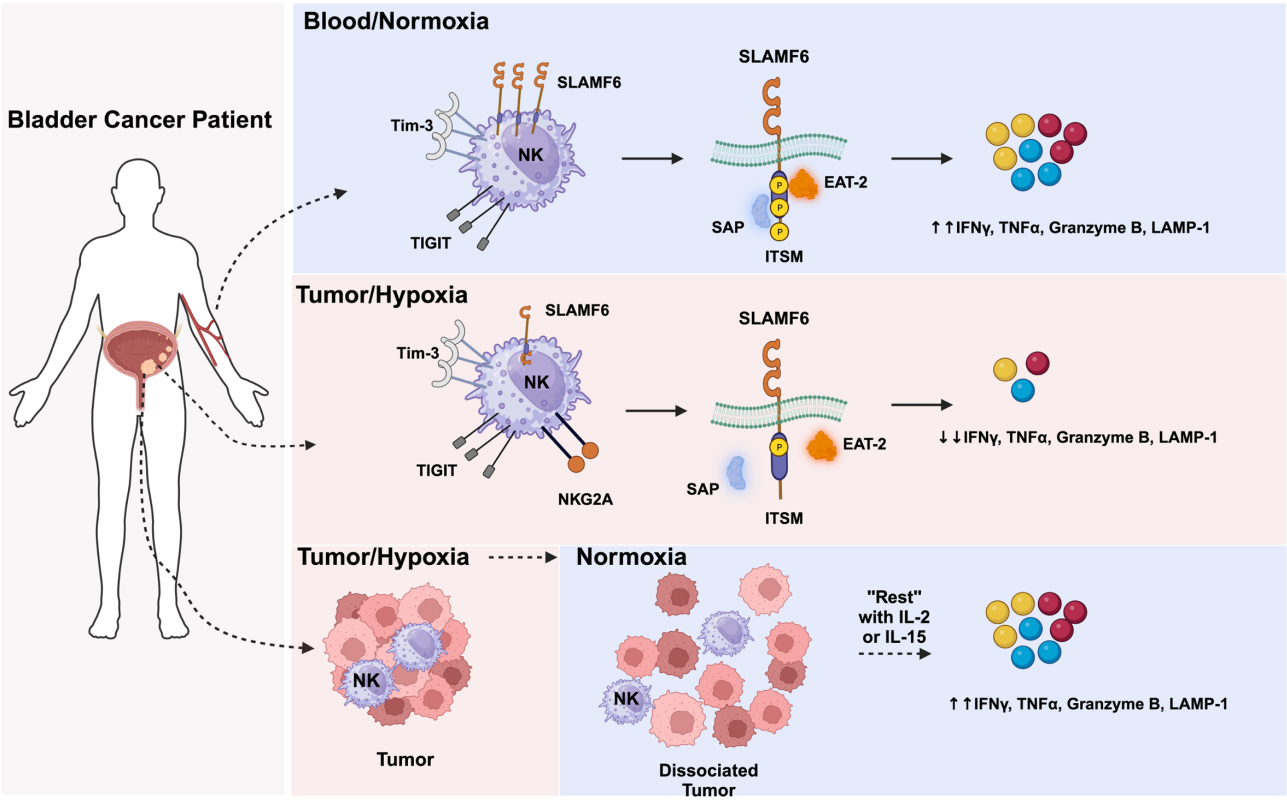

Figure 1

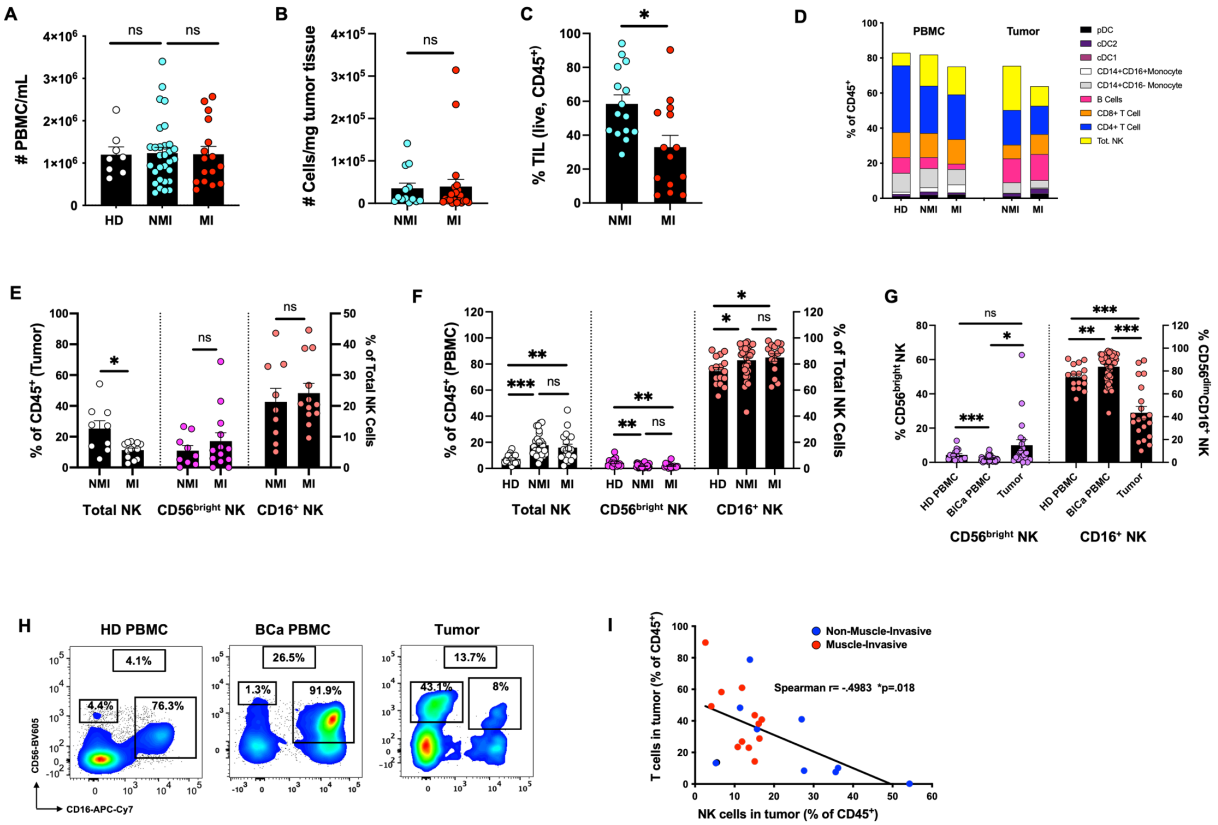

Figure 1: Bladder cancer induces NK cell maturation in peripheral blood but sustains NK cell immaturity in tumors. PBMC and cell suspensions obtained from dissociated tumor tissue were analyzed by flow cytometry to identify major immune lineages in BCa patients and HD. **(A)** Number of PBMC/mL of whole blood (HD: n=8, NMI: n= 30, MIs n= 22), **(B)** Number of viable cells/ mg of tumor tissue (NMI: n= 13, M: n= 22). **(C)** Frequency of TIL (live, CD45$^+$ cells) in NMI and MI tumors (NMI: n= 15, MI: n= 14). (**D)** Mean frequencies of major immune cell types in PBMC and TIL. **(E)** Frequency of NK cell populations in TIL expressed as a percentage of live, CD45$^+$ singlets (NMI: n= 9 , MI: n= 13). Frequencies of CD56^{bright} and CD16$^+$ sub-populations are plotted as as proportion of total NK cells on right axis. **(F)** Frequency of NK cell populations in the PBMC of HD and BCa patients (HD: n=16, NMI: n= 28, MI: n= 18). Frequencies of CD56^{bright} and CD16$^+$ sub-populations are plotted as as proportion of total NK cells on right axis. **(G)** Comparison of the frequencies of CD56^{bright}CD16$^-$ and CD56^{dim}CD16$^+$ NK cells in PBMC and tumor. **(H)** Representative FACS plots of NK cells across tissue. Boxed numbers show the frequency of NK cells amongst CD45$^+$ cells, while the percentages shown for each NK cell subset indicate the frequency amongst total NK cells. **(I)** Correlation between the frequencies of total NK cells and CD3$^+$ T cells in bladder tumors (n=22). Significance for A-G was determined by unpaired Mann-Whitney test, with ns≥.05, *p<.05, **p <.01, ***p <.001. Straight line fitting for **I** was performed using least squares regression, and significance was determined by two-tailed Spearman correlation. Error bars show S.E.M. HD=Healthy Donor, NMI=Non-Muscle-Invasive, MI=Muscle-Invasive

Figure 2

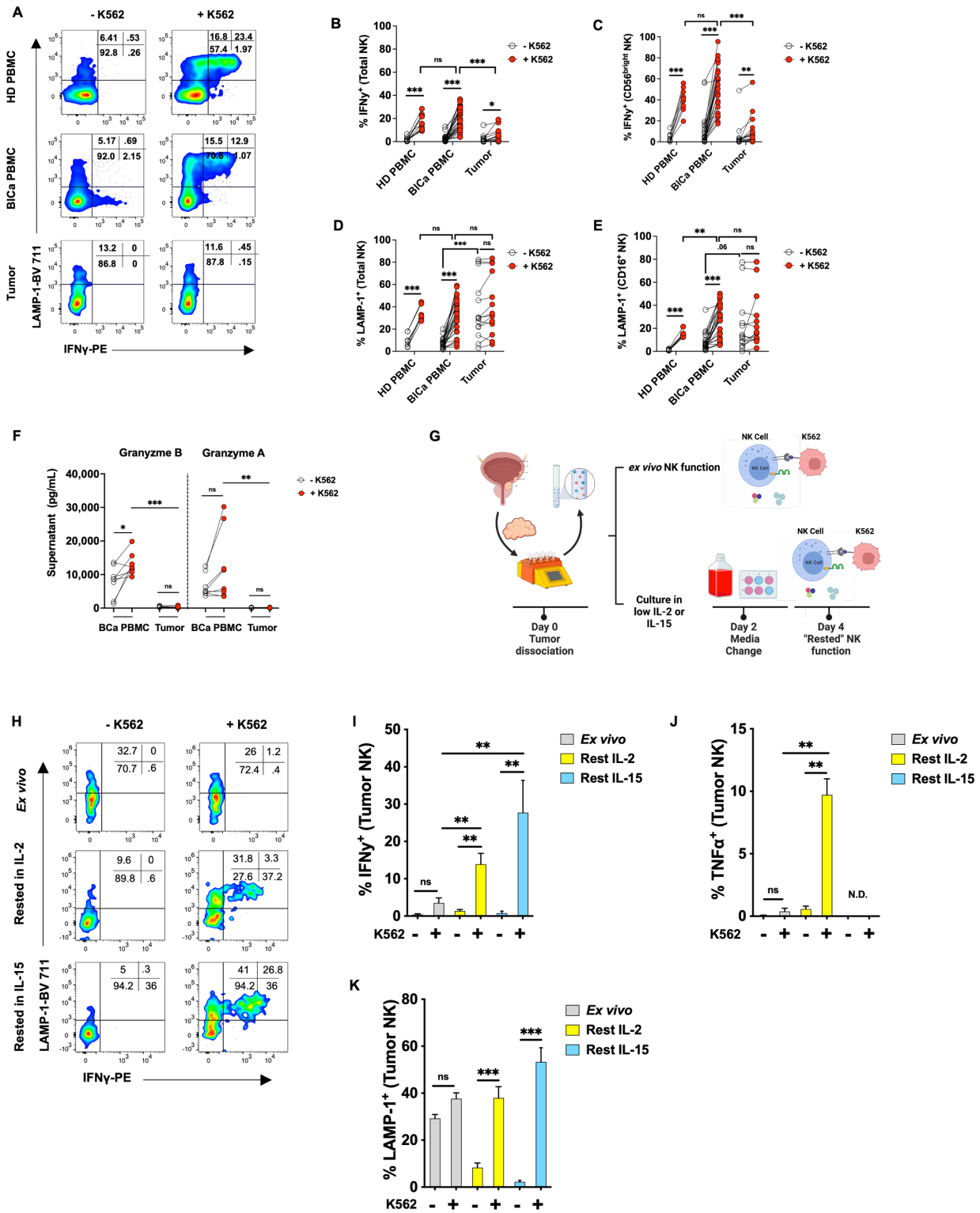

Figure 2: NK cells from the peripheral blood of BICa patients are functionally competent while tumor-infiltrating NK cells are dysfunctional, but not terminally so. PBMC or single-cell suspensions obtained from primary tumors were activated overnight with 5ng/mL of IL-15 and co-cultured ± K562 target cells to induce IFNγ and degranulation. **(A)** Representative FACS plots of LAMP-1 and IFNγ gated on total NK cells from HD and BICa patient PBMC, and from bladder tumors. **(B)** IFNγ production by total NK cells and **(C)** CD56^{bright} NK cells, (HD PBMC: n=10, BICa PBMC:

n=30, tumor: n=16). **(D)** LAMP-1 expression by total NK cells and **(E)** $CD16^+$ NK cells, (HD PBMC: n=7, BlCa PBMC: n=25, tumor: n=14).). **(F)** Granzymes B and A released into the supernatant by NK cells from BCa PBMC (n=8) or tumor (n=6) after c—culture with K562 target cells **(G)** Experimental setup for “resting’ tNK cells by culturing dissociated tumor in 50U/mL IL-2 (n=10) or 1ng/mL IL-15 (n=3) for 4 days prior to K562 co-culture. **(H)** Representative FACS plots of IFNγ and LAMP-1 gated on total tNK cells after co-culture with K562 cells directly *ex vivo* (top), or after 4d culture in the presence of IL-2 (middle) or IL-15 (bottom). Frequencies of **(I)** $IFN\gamma^+$, **(J)** $TNF\alpha^+$, or **(K)** $LAMP\text{-}1^+$ tNK cells *ex vivo* (NMI=1, MI=2), or after 4 day culture in IL-2 (NMI=5, MI=5) or IL-15 (NMI=2, MI=1). All co-cultures were stained for IFNγ and LAMP-1, but only cells rested in IL-2 were stained for TNFα. . Error bars show S.E.M. Significance was determined by t-test, with ns≥.05, *p<.05, **p <.01, ***p <.001.

Figure 3

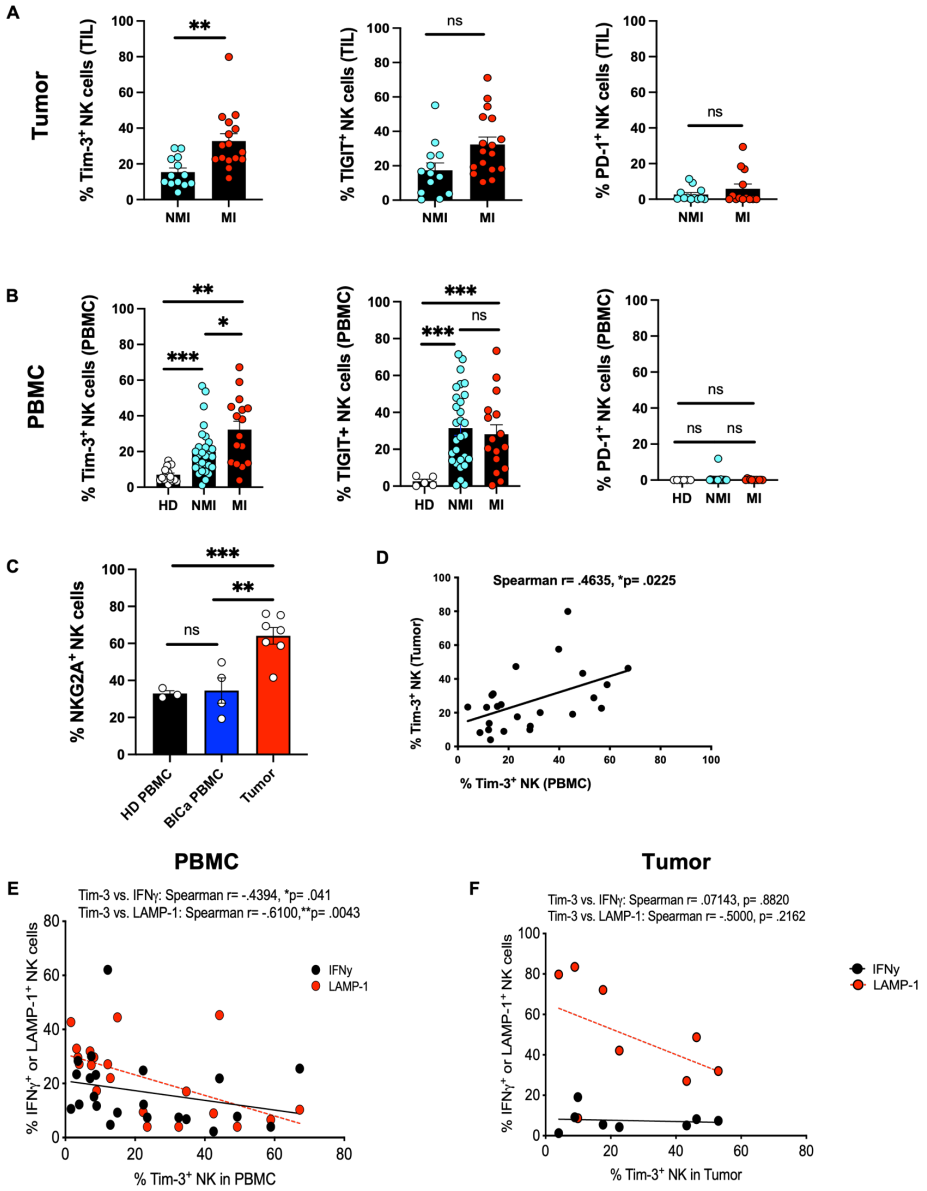

Figure 3: NK cells from BCa PBMC and tumors over-express inhibitory receptors
(A) Percentage of NK cells in tumor expressing Tim-3, TIGIT, or PD-1 (NMI: n=13, MI: n=16). **(B)** Percentage of NK cells in PBMC expressing Tim-3, TIGIT, or PD-1 (HD; n=17, NMI; n=29, MI; n=16). **(C)** Frequency of NKG2A expression on NK cells from HD PBMC (n=3) BCa PBMC (n=4) and TIL (n=7). **(D)** Correlation between the frequency of Tim-3$^+$ NK cells in the matched PBMC and tumors of 24 BCa patients. **(E)** Scatter plot showing inverse correlation between Tim-3 expression on pbNK cells and IFNγ production or degranulation (n=22). **(F)** Scatter plot showing lack of correlation between Tim-3 expression on tNK cells and IFNγ production or degranulation (n=8). Significance for A-C was determined by unpaired Mann-Whitney test, with ns≥.05, *p<.05, **p <.01, ***p <.001. Straight line fitting for **D** was performed using least squares regression, and significance was determined by two-tailed Spearman correlation. Significance for **E** + **F** was determined by two-tailed Spearman correlation. Curve-fitting (dashed line) was performed using non-linear regression and a sum of squares F test. Error bars show S.E.M. HD=Healthy Donor, NMI=Non-Muscle-Invasive, MI=Muscle-Invasive.

Figure 4

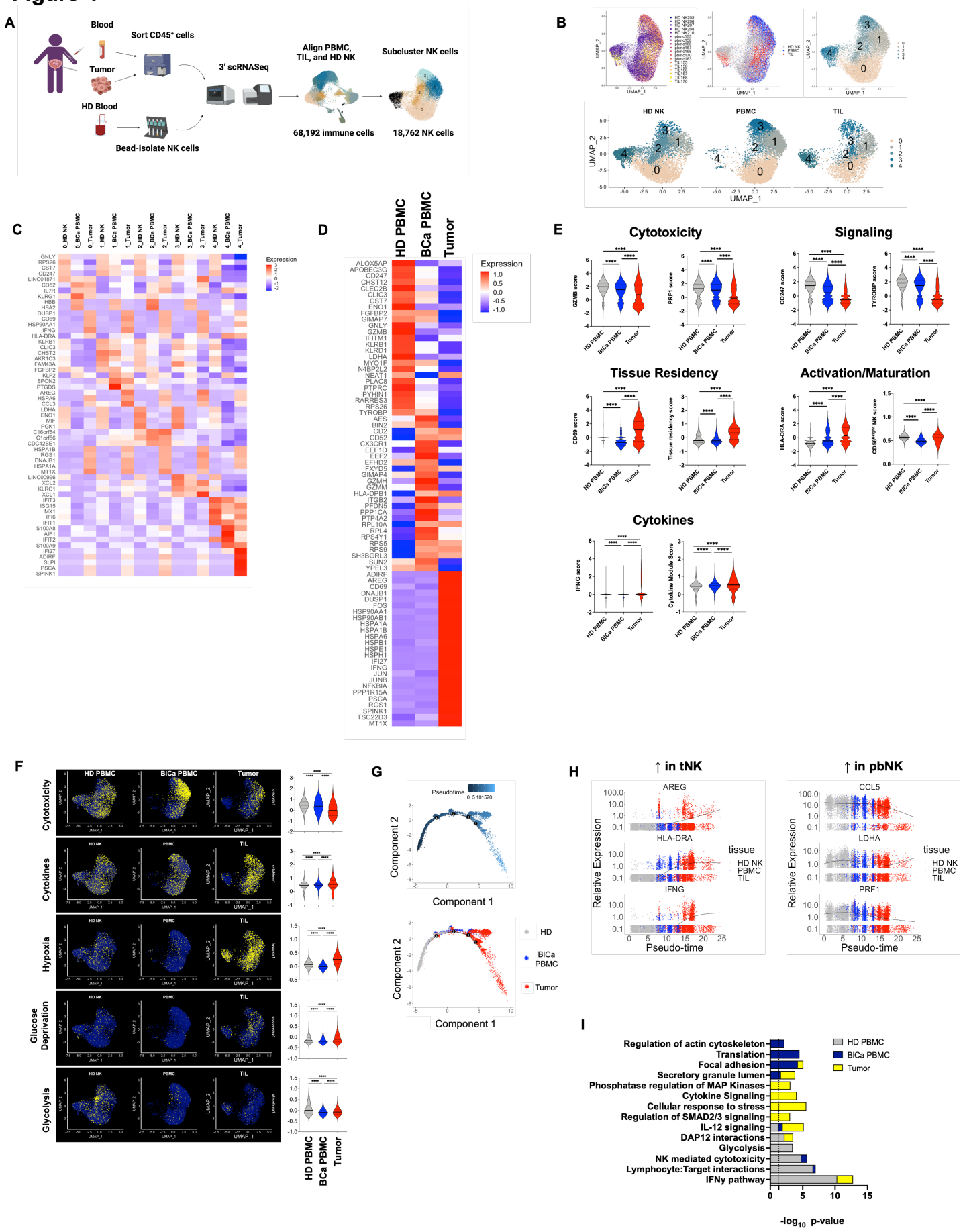
A
Blood
Sort CD45⁺ cells
Tumor
HD Blood
Bead-isolate NK cells
3' scRNASeq
Align PBMC, TIL, and HD NK
68,192 immune cells
Subcluster NK cells
18,762 NK cells
B
HD NK
PBMC
TIL
UMAP_1
UMAP_2
C
Expression
D
HD PBMC
BCa PBMC
Tumor
Expression
E
Cytotoxicity
Signaling
Tissue Residency
Activation/Maturation
Cytokines
HD PBMC
BlCa PBMC
Tumor
F
Cytotoxicity
Cytokines
Hypoxia
Glucose Deprivation
Glycolysis
HD PBMC
BCa PBMC
Tumor
G
Pseudotime
Component 1
Component 2
HD
BlCa PBMC
Tumor
H
↑ in tNK
↑ in pbNK
AREG
HLA-DRA
IFNG
CCL5
LDHA
PRF1
Relative Expression
Pseudo-time
tissue
HD NK
PBMC
TIL
I
Regulation of actin cytoskeleton
Translation
Focal adhesion
Secretory granule lumen
Phosphatase regulation of MAP Kinases
Cytokine Signaling
Cellular response to stress
Regulation of SMAD2/3 signaling
IL-12 signaling
DAP12 interactions
Glycolysis
NK mediated cytotoxicity
Lymphocyte:Target interactions
IFNγ pathway
HD PBMC
BlCa PBMC
Tumor
-log10 p-value

Figure 4: Distinct programs of gene expression define NK cells across tissue and disease state. (A) Total PBMC (NMI; n=2, MI; n=5) and patient-matched $CD45^+$ TIL (NMI; n=2, MI; n=4) were FACS sorted and sequenced for 3' scRNASeq usings the 10x platform. The resulting clusters were integrated with scRNASeq libraries generated from NK cells in HD PBMC (n=5) to allow comparisons across tissue and disease-state. **(B)** UMAP depicting 18,762 sub-clustered NK cells derived from bladder tumor, PBMC from BlCa patients, or HD PBMC. Clusters are colored by donor, tissue of origin, and cluster (top panel), and cluster membership separated by tissue (bottom panel). **(C)** Heatmap showing scaled expression of the top 5 significant DEG by cluster and tissue of origin, ordered by adjusted p-value, in pbNK cells from HD and pbNK and tNK cells from BCa patients. **(D)** Heatmap showing scaled expression of the top 25 significant DEG by tissue of origin, ordered by adjusted p-value, in pbNK cells from HD and pbNK and tNK cells from BCa patients. **(E)** Scaled expression of the indicated genes or gene signatures in NK cells from the indicated tissues. **(F)** Single-cell module scores for gene signatures pertaining to metabolic and immune processes across tissue of origin overlaid on UMAP plots (left) and quantified (right). For UMAP plots, non-zero expression between the 10th and 90th quantiles is shown. **(G)** Single-cell trajectory of NK cells colored by pseudotime (top) and by tissue of origin (bottom). **(H)** Expression of select genes as a function of pseudotime. **(I)** Select Gene Ontology and KEGG terms enriched in NK cells from peripheral blood or tumor. For violin plots, median expression (solid line) and quartiles (dotted lines) are shown with significance calculated using an unpaired Mann-Whitney t-test ($p \geq .05$, $^*p<.05$, $^{**}p<.01$, $^{***}p<.001$, $^{****}p<.0001$). Significant differential gene expression was performed in Seurat using a non-parameteric Wilcoxon rank sum test. Pathway enrichment analysis was performed with Enrichr using Fisher's exact test.

Figure 5

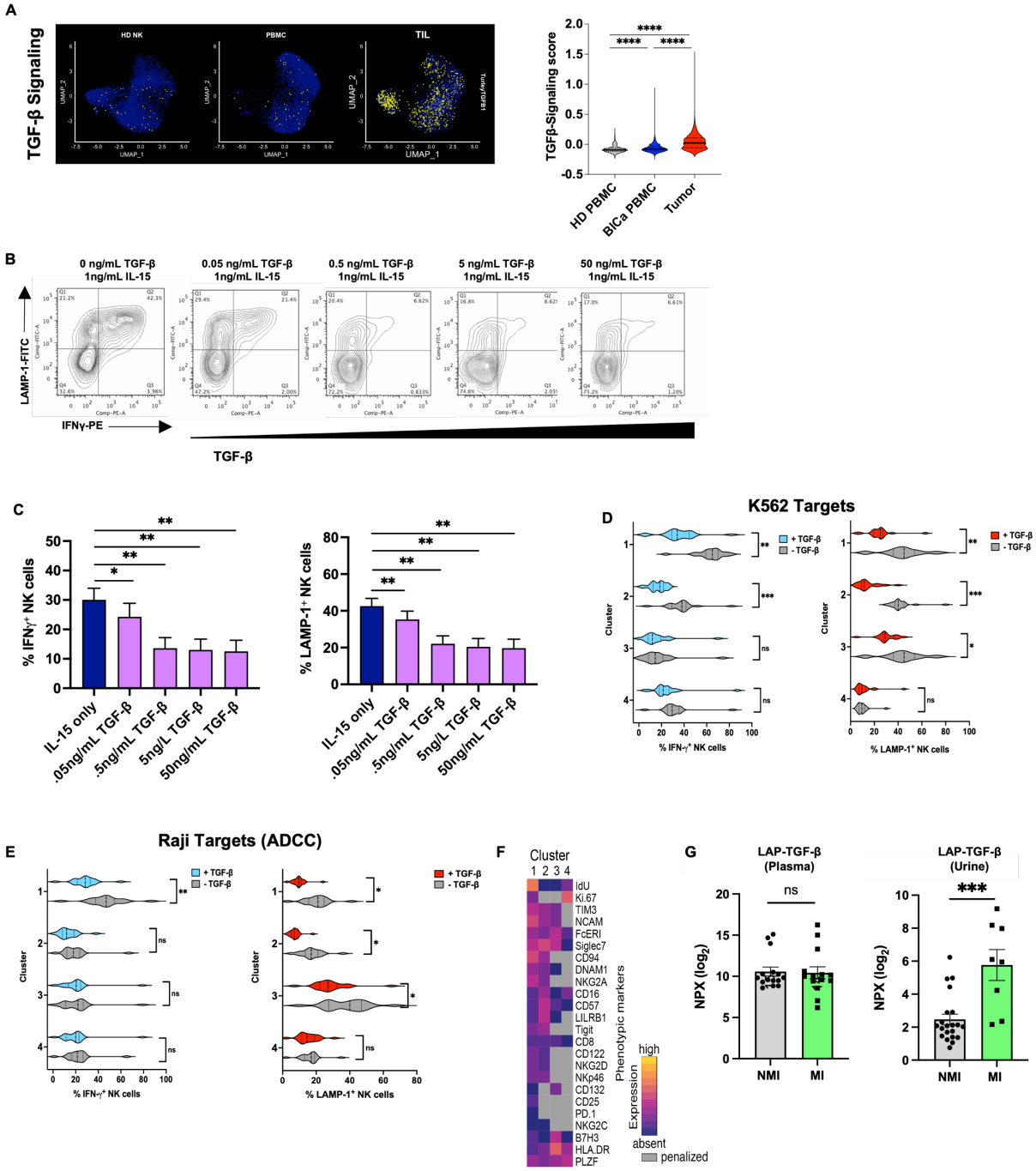

Figure 5: TGF-β in the TME suppresses NK cell function. (A) Single-cell module score for a TGF-β signaling signature overlaid on UMAP plots of pbNK cells from HD and BCa patients, or tNK cells (left) and quantified (right). For UMAP plots, non-zero expression between the 10th and 90th quantiles is shown. HD NK cells (n=6) were bead-isolated from PBMC and cultured for 6 days in the presence of 1ng/mL IL-15 alone or in combination with increasing concentrations of TGF-β (.05ng/mL-50ng/mL), before K562 target cell co-culture and FACS. **(B)** Representative FACS plots for IFNγ and LAMP-1. **(C)** Frequency of IFNγ+ and LAMP-1+ NK cells from day 6 for IL-15 ± TGF-β-treated NK cells. **(D)** HD PBMC (n=20 donors) were cultured with 1ng/mL IL-15 or IL-15 and 5ng/mL TGF-TGF-β, for 6 days, analyzed by CyTOF, and clustered with Depeche. Comparison of IFNγ production and LAMP-1 expression, with or without TGF-β, for each cluster was performed. **(E)** HD NK cells (n=20) were cultured as above, but anti-CD20 coated Raji cells were used as targets to assess function

elicited by ADCC. Comparison of IFNγ production and LAMP-1 expression, with or without TGF-β, for each cluster was performed. **(F)** Protein-level expression of markers for each cluster as determine by CyTOF. **(G)** Olink analysis of soluble proteins was performed on BCa patient plasma (NMI=15, MI=14) and cell-free patient urine (NMI=21, MI=8). Significance was calculated using paired t-test for **C** and unpaired Mann-Whitney t-test for **G.** Error bars show S.E.M .Significance for CyTOF was performed by . . . . . (p≥.05, *p<.05, **p <.01, ***p <.001, ****p <.0001).

Figure 6

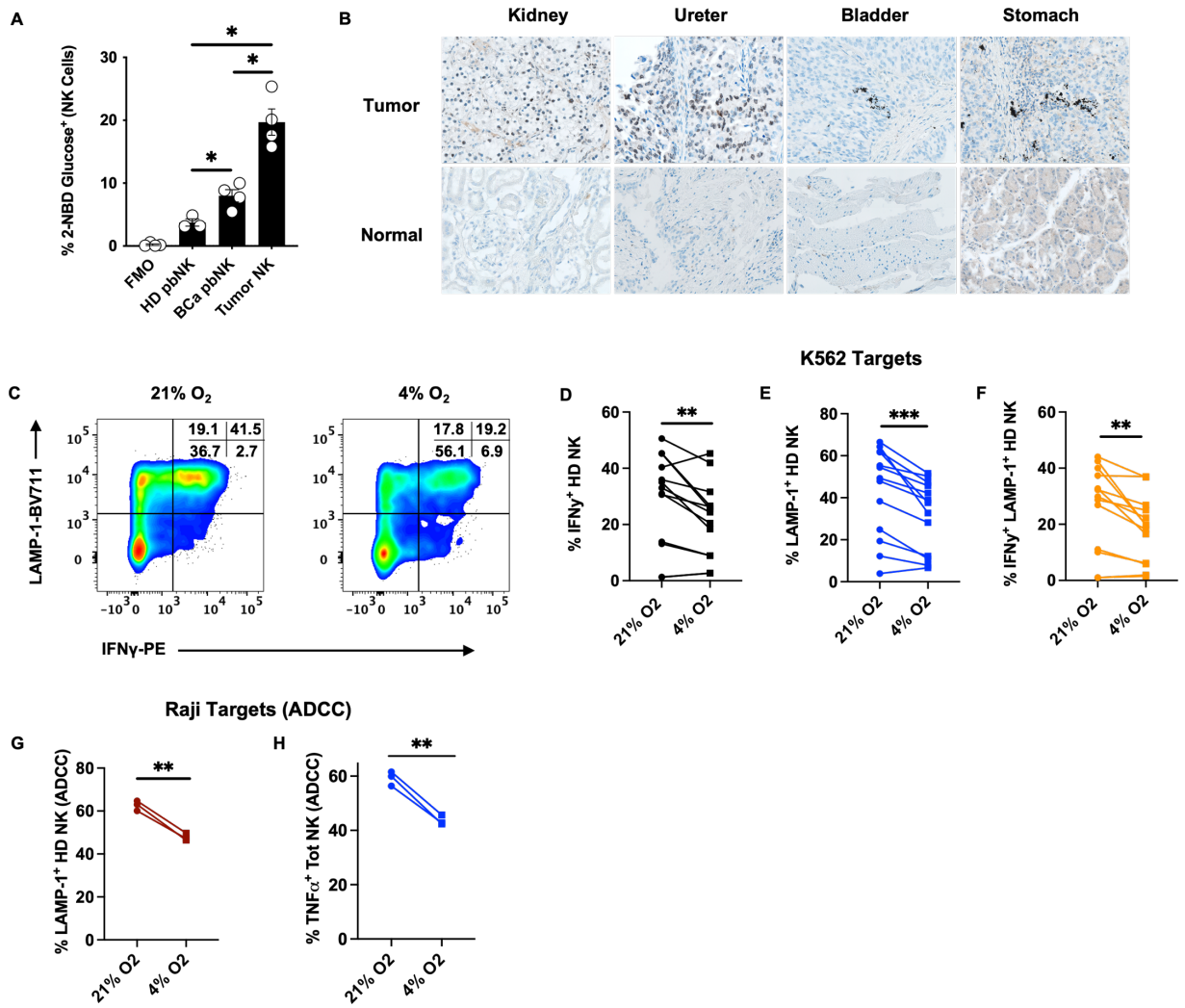

Figure 6: Hypoxia suppresses NK cell function. PBMC from HD (n=3), BCa patients (n=4) or dissociated tumor (n=4) were incubated with the fluorescent glucose analog 2-NBDG-FITC to determine glucose uptake, then stained with FACS antibodies to identify NK cells by flow cytometry. **(A)** Percentage of 2-NBDG$^+$ NK cells. **(B)** FFPE sections of kidney, ureter, bladder, and stomach tumors, as well as normal tissue from those organs (unmatched), was stained for HIF-1α (brown) and hematoxylin (blue). Images are magnified 63x and representative of two independent experiments. **(C)** Representative FACS plots of IFNγ and LAMP-1 on HD NK cells cultured for 3 days under normoxic (21% O_2) or hypoxic (4% O_2) conditions prior to co-culture with K562 targets. **(D)** Frequencies of IFNγ$^+$, **(E)** LAMP-1$^+$, or **(F)** IFNγ$^+$LAMP-1$^+$ HD NK cells (n=13) after 3-4 days of normoxic or hypoxic culture followed by co-culture with K562 target cells. **(G)** ADCC-induced expression of LAMP-1 and **(H)** TNFα by HD NK cells (n=3) in response to anti-CD20 and co-culture with Raji cell targets after 4 days of normoxic or hypoxic culture. Significance was calculated using unpaired t-test for **A** and paired t-test for **D-H** with error bars showing S.E.M. and p≥.05, *p<.05, **p <.01, ***p <.001, ****p <.0001.

Figure 7

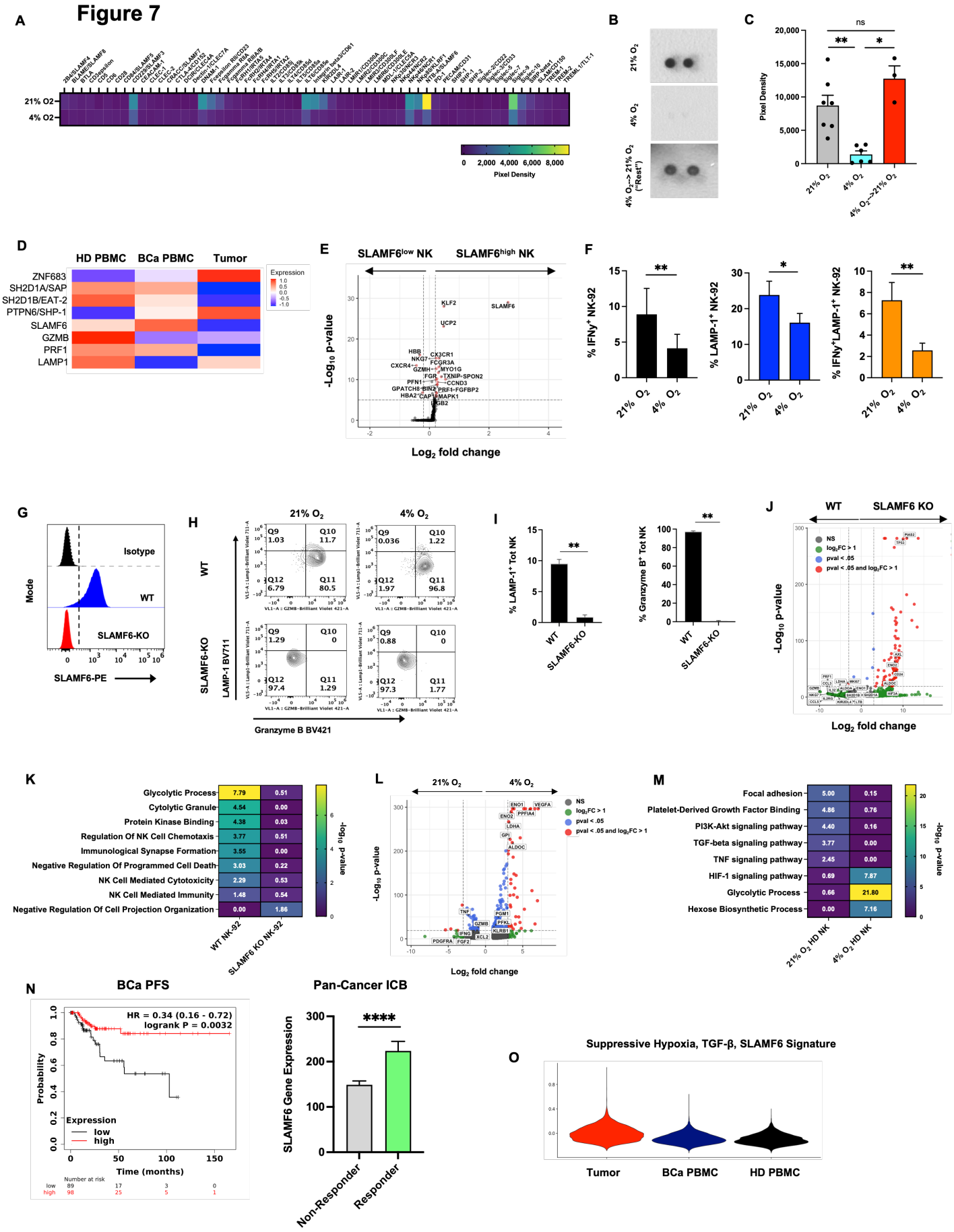
A
21% O2
4% O2
Pixel Density
B
21% O2
4% O2
4% O2--> 21% O2 ("Rest")
C
ns
**
*
Pixel Density
21% O2
4% O2
4% O2-->21% O2
D
HD PBMC
BCa PBMC
Tumor
ZNF683
SH2D1A/SAP
SH2D1B/EAT-2
PTPN6/SHP-1
SLAMF6
GZMB
PRF1
LAMP1
Expression
E
SLAMF6low NK
SLAMF6high NK
-Log10 p-value
Log2 fold change
KLF2
SLAMF6
UCP2
F
% IFNγ+ NK-92
% LAMP-1+ NK-92
% IFNγ+LAMP-1+ NK-92
21% O2
4% O2
G
Mode
Isotype
WT
SLAMF6-KO
SLAMF6-PE
H
21% O2
4% O2
WT
SLAMF6-KO
LAMP-1 BV711
Granzyme B BV421
I
% LAMP-1+ Tot NK
% Granzyme B+ Tot NK
WT
SLAMF6-KO
J
WT
SLAMF6 KO
NS
log2FC > 1
pval < .05
pval < .05 and log2FC > 1
-Log10 p-value
Log2 fold change
K
Glycolytic Process
Cytolytic Granule
Protein Kinase Binding
Regulation Of NK Cell Chemotaxis
Immunological Synapse Formation
Negative Regulation Of Programmed Cell Death
NK Cell Mediated Cytotoxicity
NK Cell Mediated Immunity
Negative Regulation Of Cell Projection Organization
WT NK-92
SLAMF6 KO NK-92
-log10 p-value
L
21% O2
4% O2
NS
log2FC > 1
pval < .05
pval < .05 and log2FC > 1
-Log10 p-value
Log2 fold change
M
Focal adhesion
Platelet-Derived Growth Factor Binding
PI3K-Akt signaling pathway
TGF-beta signaling pathway
TNF signaling pathway
HIF-1 signaling pathway
Glycolytic Process
Hexose Biosynthetic Process
21% O2 HD NK
4% O2 HD NK
-log10 p-value
N
BCa PFS
HR = 0.34 (0.16 - 0.72)
logrank P = 0.0032
Probability
Expression
low
high
Time (months)
Number at risk
Pan-Cancer ICB
****
SLAMF6 Gene Expression
Non-Responder
Responder
O
Suppressive Hypoxia, TGF-β, SLAMF6 Signature
Tumor
BCa PBMC
HD PBMC

Figure 7: NK cell dysfunction in the TME results from a hypoxia-induced suppression of signaling through SLAMF6. (A) Densitometry quantification of tyrosine phosphorylation in the ITAM/ITIM/ITSM of 59 immune receptors on HD NK cells after 4 days of normoxic (n=5) or hypoxic culture (n=4). **(B)** Representative blot showing tyrosine phosphorylation on the ITSM of SLAMF6 in HD NK cells after 3-4 days of normoxic or hypoxic culture, or 3 days of hypoxic culture followed by 3 days of normoxic culture ("Rest"). **(C)** Densitometry quantification of tyrosine phosphorylation on the ITSM of SLAMF6 in HD NK cells after 3-4 days of normoxic (n=8) or hypoxic culture (n=6), or 3 days of hypoxic culture followed by 3 days of normoxic culture ("Rest") (n=3). **(D)** Single-cell expression of genes involved in SLAMF6 signaling as well as genes for effector function in pbNK from HD and BCa patients, and tNK cells. **(E)** Volcano plot showing enrichment of effector gene expression in SLAMF6^{high} versus SLAMF6^{low} NK cells from scRNAseq (HD PBMC: n=5, BCa PBMC: n=7, Tumor: n=6). Expression of >1 was used as the threshold for SLAMF6^{high} NK cells. **(F)** Frequencies of for IFNγ^{+}, LAMP-1^{+}, or IFNγ^{+}LAMP-1^{+} NK-92 cells (n=3) after 3-4 days of normoxic or hypoxic culture and co-culture with K562 target cells. **(G)** Representative histograms showing SLAMF6 expression in WT NK-92 and RNP CRISPR-generated SLAMF6-KO NK-92 cells (n=5). **(H)** Representative FACS plots of LAMP-1 and Granzyme B expression in WT or SLAMF6-KO NK-92 cells after 3 days of normoxic or hypoxic culture followed by co-culture with K562 target cells. **(I)** Expression of Granzyme B and LAMP-1 by WT or SLAMF6-KO NK-92 cells after co-culture with K562 targets. Data are from two independent experiments. **(J)** Bulk RNAseq of WT or SLAMF6-KO NK-92 cells showing an enrichment of effector gene expression in WT cells compared to SLAMF6-KO. **(K)** Select Gene Ontology or KEGG terms significantly enriched in WT and SLAMF6 KO NK-92 cells. The top 100 significant DEG were used as input. **(L)** Bulk RNAseq of HD NK cells cultured at 21% or 4% O_2 for 3 days. **(M)** Select Gene Ontology or KEGG terms significantly enriched in HD NK cells cultured at 21% or 4% O_2 for 3 days. The top 100 significant DEG were used as input**.** **(N)** PFS for BCa patients stratified by high or low SLAMF6 gene expression as determined by bulkRNAseq (kmplot.com, n=187). **(O)** Expression of a gene signature comprised of inhibitory SLAMF6 pathway genes, hypoxia, and TGF-β signaling transcripts (Table S4) in scRNASeq of NK cells from the indicated tissues. Response to ICB stratified by SLAMF6 expression across 13 solid tumors in a cohort of 1,160 patients (kmplot.com). ITAM/ITIM/ITSM= Immunoreceptor Tyrosine Activating/Inhibitory/Switch Motif. PFS= Progression Free Survival, ICB= Immune Checkpoint Blockade Error bars show S.E.M. ns ≥.05 *p<.05, **p <.01, ***p <.001, ****p <.0001 as determined by unpaired or paired t-test.